SULFATE ATTACK RESISTANCE OF ECO-EFFICIENT CEMENT-BASED MORTAR MIXTURES

Islam Orynbassarov, B. Eng.

**Submitted in fulfilment of the requirements for
the degree of Master of Science
in Civil & Environmental Engineering**

NAZARBAYEV UNIVERSITY

**School of Engineering and Digital Sciences
Department of Civil & Environmental Engineering
Nazarbayev University**

53 Kabanbay Batyr Avenue,
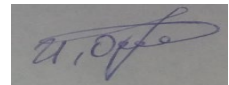Nur-Sultan, Kazakhstan, 010000

Supervisors: Jong Ryeol Kim & Chang-Seon Shon

March 2021

Declaration

I hereby, declare that this manuscript, entitled "sulfate attack resistance of eco-efficient cement-based mortar mixtures", is the result of my own work except for quotations and citations which have been duly acknowledged.

I also declare that, to the best of my knowledge and belief, it has not been previously or concurrently submitted, in whole or in part, for any other degree or diploma at Nazarbayev University or any other national or international institution.

Islam Orynbassarov

04.05.2021

Abstract

Ordinary Portland cement (OPC) is one of the most widely used construction materials in civil engineering infrastructure construction but it is susceptible to sulfate attack. One of the ways to improve the sulfate resistance of an OPC mortar/concrete is to replace a certain amount of OPC with different pozzolanic materials such as ground granulated blast furnace slag (GGBFS) and metakaolin. The use of pozzolanic materials to mortar/concrete not only enhances durability but also reduces carbon dioxide (CO_2) emission due to the less usage of OPC at the initial construction state. As considering these aspects, limestone calcined clay cement (LC3) has been developed in recent decades. However, the influence of LC3 on sulfate attack resistance has not been fully evaluated. Therefore, this study investigated the efficiency of LC3 mortar mixtures against sulfate attack in normal and wet-dry cycle exposure conditions up to approximately 6 months. To evaluate the synergistic effect of a combination of LC3 and GGBFS on the sulfate resistance, the LC3 and OPC mixtures containing 25% and 50% GGBFS were also assessed. Three different initial curing periods, namely 1-day, 3-day, and 16-d warm curing, were applied to both LC3 and GGBFS-incorporated LC3 mixtures in order to achieve similar sulfate testing strength to OPC mixtures. Therefore, the initial compressive strength of LC3 mixtures with/without GGBFS for measuring the volumetric expansion of mixtures submersed into 5% sodium sulfate (Na_2SO_4) solution was categorized into 3 MPa, 7 MPa, and 14 MPa. To further examine the properties of LC3 mixtures, density, porosity, compressive strength, weight changes, and dielectric constant tests were conducted. The experiment results show that the expansion of the LC3 mixture with initial strength of under 7 MPa regardless of the addition of GGBFS and initial curing made a plateau after a rapid increase up to 7 days, while the expansion of the OPC mixture kept increasing throughout the period. The LC3 mixtures demonstrated negligible expansions with the initial high strength of approximately 14 MPa under fully submersed test condition. However, in the wet-dry cycle condition, the LC3 mixture is discovered to be more susceptible than OPC at both low and high strength. Furthermore, the addition of GGBFS to OPC or LC3 mixture provides the synergistic effect on reducing the expansion due to sulfate attack. Therefore, if the LC3 mixture has high initial strength (min. 15 MPa) and dense microstructure to minimize the penetration of sulfate ion into the mixture, it is expected that the LC3 mixture is more efficient than the OPC mixture against the sulfate attack.

Acknowledgements

I would first like to take this opportunity to thank all the people who assisted me to do this work. Especially, my genuine thanks go to one of my thesis supervisors, Assistant Professor Chang-Seon Shon, for accepting me as one of his graduate students, and for his invaluable advice and feedback throughout the research. Furthermore, he provided me with sufficient support in terms both financially and materially. I am definitely grateful for every minute of the meetings that he spent.

Next, I should also thank Professor Kim who accepted me to work in the laboratory and supported me financially. I convey my special thanks to Umut Bektimirova and Aidyn Tugelbayev who assisted me with lab work. I also express my genuine appreciation to the laboratory assistants who helped me when I asked.

Finally, I express my appreciation to my family for their love, care, and prayers. I am grateful to them for their permanent support in everything.

Table of Contents

List of Abbreviations

CH	Calcium hydroxide
CSH	Calcium silicate hydrate
FA	Fly ash
GGBFS	Ground granulated blast furnace slag
GPR	Ground penetration radar
LC3	Limestone calcined clay cement
OPC	Ordinary Portland cement
RDC	Relative dielectric constant
SCMs	Supplementary cementitious materials
SF	Silica fume
TSA	Thaumasite sulfate attack

List of Figures

List of Tables

Chapter 1 – Introduction

1.1 Background

Recently, a great deal of attention has been paid to the environmental issues associated with waste pollution and high energy consumption, resulting in the release of a large amount of greenhouse gases, specifically carbon dioxide. It is well known that almost all countries have signed the Paris Agreement to decrease the growing level of man-made carbon dioxide emissions that is the main cause of global warming (Farfan et al., 2019). To achieve zero carbon emissions to some extent, many countries are setting their goals in the near future. Although power generation is comparatively achievable with obligation and engagement thanks to technological advancement in alternative energy sources, the case with the cement industry is different since it consumes, the critical core material of clinker production, limestone that is the source of greenhouse gas.

Concrete is believed to be the second most utilized substance after water (Ramezanianpour, 2012) but the most consumed construction material, being manufactured in the amount of about 3-3.8 tonne per person annually (Crossin, 2015). Therefore, it is currently considered that cement manufacturing is the global economy's second carbon-polluting industry only after steel manufacturing and has responsibility for around 5-8% of global carbon dioxide (CO_2) emissions (Farfan et al., 2019; Lu & Poon, 2018; Sharp et al., 2010; Summerbell et al., 2016; Xie et al., 2011). However, this may not be the highest limit of pollution since developing countries are still expanding their production capacity and implementing huge engineering projects. Some studies have forecasted the level of carbon pollution to increase further by 111% by the year 2030 comparing to before 2005 (Summerbell et al., 2016). If take a look at the history of cement production, the capacity of production has recently increased by 25 times in comparison with the scale of the 1950s (Farfan et al., 2019). During the period of 2011 to 2013, for example, giving off an additional 3.2 Gt of CO_2 equivalent into the atmosphere, China manufactured and used 3.8 Gt of cement that is more than the USA consumed during the 20th century (Farfan et al., 2019).

It has been well established that OPC is manufactured by mixing row materials, namely iron ore, limestone as a source of calcium and clay as a source of silica and alumina at more than 1450ºC in a rotary kiln requiring an enormous amount of heat to achieve the chemical reactions that turn the initial raw materials into clinker (Ramezanianpour, 2012). Consequently, that leads to a large amount of carbon dioxide. According to the recent studies (Farfan et al.,

2019; Özbay et al., 2016; Summerbell et al., 2016) about the carbon dioxide sources in clinker manufacturing, around 50% of carbon emissions come from materials (roughly 525 kg CO_2/tonne of clinker), 40% of them fuel-derived (roughly 335 kg CO_2/tonne of clinker) while only 10% are generated by electricity and transportation equally. However, that is influenced by several reasons such as technological process, energy, and fuel origin, filtering mechanisms, and geography (Farfan et al., 2019). The inevitable thermal treatment process of limestone ($CaCO_3$) to produce lime (CaO), which is the main ingredient for cement clinker, could be an example of a source of carbon emission (CO_2) generated by materials (Farfan et al., 2019; Summerbell et al., 2016). In accordance with the authors, the process with limestone produces a similar amount of carbon dioxide as when burning coal.

The popular ways to decrease the greenhouse gas emissions and to maintain sustainable economic growth in terms of the cement industry consists of general three approaches such as energy efficiency in the processes during the production, alternative and sustainable fuels, and replacement of cement clinker with other eco-efficient materials (Crossin, 2015). Citing Madlool et al., Summerbell et al. (2016) reported that using some current beneficial technologies can save the utilized energy between 100 MJ and 1400 MJ per tonne of product, thus cutting costs starting from around 2% at worse and approximately 40% at best depending on many factors such as types and installation costs of technologies and countries.

The same paper, however, argues such an improvement stating some present obstacles like high and risky initial costs and unproven results of technology, lack of enough money to invest, and the unforeseen situation in the economy. For example, if there is cheap energy it will decrease the importance of investment, and in the case of expensive energy that will make it harder to compete with imports coming from cheap energy countries. In addition, others think that today's state-of-the-art processes of Portland cement production consuming fossil fuels has almost come to the end of its energy effectiveness (Sharp et al., 2010).

However, the third way to reduce carbon footprint in cement and concrete industries is to use supplementary cementitious materials (SCMs) such as ground granulated blast furnace slag (GGBFS), silica fume, fly ash, pozzolans, and metakaolin and to use different types of cement connected to low carbon release. For example, as a better way for decreasing the carbon dioxide release of modern OPC industry, several solutions have been suggested such as (Sharp et al., 2010):

    i.   Adding powders of limestone and some different "reactive fillers"

    ii.   Blending "latent hydraulic materials" (GGBFS)

    iii.   Using "pozzolanic materials" like natural pozzolans and fly ash

In this study, therefore, these options are considered as eco-efficient binders and investigated. As stated by (Ramezanianpour, 2012), the application of SCMs has expanded over the years from 10% (1990) to 15% (2005) with a predicted increase in the future. Making a high volume of GGBFS blended cement with 50%, 60%, 70%, and 80% replacement of Portland cement clinker and adding them to concrete is one of the best ways to reduce environmental pollution, for example. That, in turn, solves to some extent not only carbon emission that comes from a high power-consuming OPC production but also a waste disposal problem from the metallurgical industry. For example, Shi and Qian (2000) reported that 4000 MJ of energy is used to produce a ton of cement, and replacement of clinker with industrial slag saves about 90% of the energy used for OPC production. Moreover, the replacement of GGBFS with clinker provides improved quality in many situations in a long term such as good strength development and sulfate resistance thanks to its small particle size distribution and pore refinement.

Despite such good properties of SCMs such as GGBFS in the replacement of Portland cement clinker, there is a barrier in the wide use of slag. For instance, currently, just about one-fifth of cement clinker on average is replaced by SCMs such as GGBFS, fine limestone, and coal fly ash (K. L. Scrivener et al., 2018). According to the paper, the limit is related to the availability of such materials worldwide in the amount of approximately 15-20% compared to the cement manufacturing. Also, since the sources of the SCMs are heavy industries such as iron ore and coal production, not all countries have enough quantity of resources and they are expected to decrease in capacity in the future due to the sustainability concerns and reuse of wastes (K. Scrivener et al., 2018).

Therefore, the use of one of the richest resources around the world, clay, is proposed as a solution for sustainable growth. A combination of the calcined clay with limestone, gypsum, and clinker gives a promising new type of cement as known limestone calcined clay cement (LC3). Depending on its replacement level and chemical composition, the cement has demonstrated a comparable characteristic with OPC in terms of durability, physical and mechanical properties.

For instance, there are several studies about the physical and mechanical properties of LC3 cement. Some have tried to examine the durability aspects such as chloride ion ingress and carbonation (Yuvaraj Dhandapani et al., 2018; Maraghechi et al., 2018; K. Scrivener et al., 2018) and few papers about sulfate resistance of LC3 (Z. Shi et al., 2019) following the minimum strength requirements of ASTM standard in normal condition. However, it is not always possible to cure concrete structures until they get the required minimum strength.

1.2 Research Objectives and Scopes

Even though a lot of work has been done by many researchers to investigate the durability performance of OPC, LC3 systems have not been fully evaluated because of their comparatively recent development. Particularly, there are fewer data available in terms of sulfate attack resistance of LC3 and LC3 mixtures containing GGBFS compared to mixtures made from OPC.

In this study, therefore, the efficiency of mortar mixtures made from ordinary Portland cement, LC3, and GGBFS with various proportions against sulfate attack were investigated from comprehensive laboratory test programs. These include density, porosity, compressive strength, drying shrinkage, weight changes, volumetric sulfate expansion, and dielectric constant tests. Other test parameters include three different curing regimes to obtain different initial strength of the mixtures which were exposed to 5% sodium sulfate (Na_2SO_4) solution, with normal and wet-dry cycle conditions up to approximately 6 months. Furthermore, based on the obtained results from laboratory tests and their consequent analysis, the relationships between expansion due to sulfate attack and different testing parameters such as porosity, density, compressive strength, weight change, and dielectric constant values were examined. After that, all necessary correlations that may explain the resistance of all mortar mixtures (OPC, OPC containing GGBFS, LC3, and LC3 incorporating GGBFS) to sulfate attack were identified

1.3 Thesis structure

This work consists of five chapters. In the first chapter, the main general information about the research background, the worthiness of the selected study, the problems and objectives of the investigation along a thesis structure are provided. The second chapter discusses the existing work done by previous researchers. In other words, the literature review tries to evaluate the main features of LC3 and GGBFS comparing with OPC. Moreover, the determination of dielectric properties of mixtures along with a working mechanism is explained. Finally, and most importantly, durability characteristics mainly focusing on types, mechanisms, and consequences of sulfate attack are discussed.

In chapter three, the main physical and chemical characteristics of materials, the experiment design indicating specific test methods followed during the research, mixture proportions, and curing conditions of samples are presented. The fourth chapter shows the analysis of results and provides the related discussions. In the last chapter, as a conclusion, the main findings and limitations are summarized and future recommendations are also provided.

Chapter 2 – Literature Review

2.1 Ground Granulated Blast Furnace Slag (GGBFS)

2.1.1 Background

Blast furnace slag is a secondary product generated in the amount of 260-300 kg per tonne of the pig-iron during the reaction between ignition residue, impurities and a chemical cleaning agent called flux (Crossin, 2015) when slagging agents such as Limestone or Dolomit and a reducing agent such as coke are added to the iron ore to remove the impurities at the temperature of 1400-1600°C (see Figure 2.1) (Li et al., 2010; Özbay et al., 2016). According to Crossin (2015), the gained material needs then to be processed with two various techniques depending on the final product. Firstly, it can be treated by air-cooling to get low-class materials usually used in bitumen as aggregate. The second method implies using water as a cooler to obtain granulated blast furnace slag which, with the addition of gypsum and pulverizing it, can be further converted to ground granulated blast furnace slag.
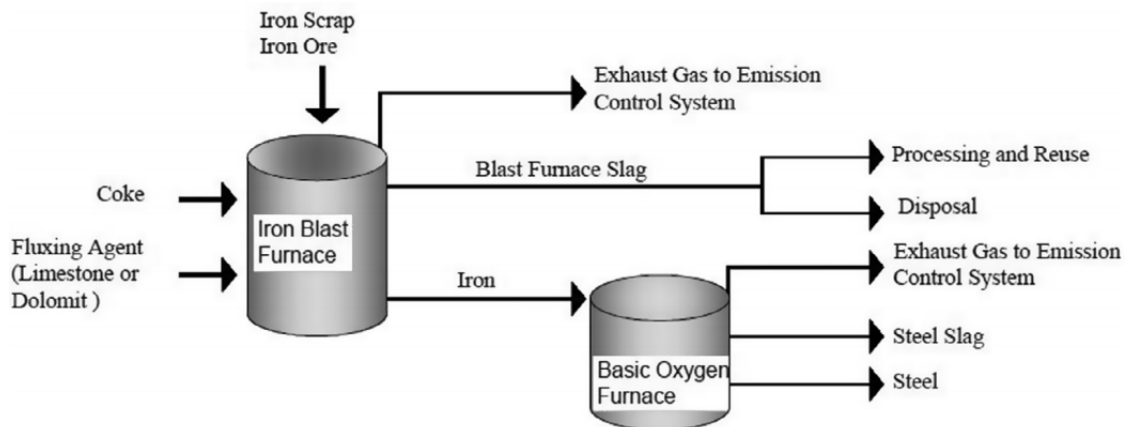
Figure 2.1: The process of slag production (Özbay et al., 2016).

Ground granulated blast furnace slag (GGBFS) is a glassy granular by-product of pig iron and steel fabrication and obtained from blast-furnace by cooling it with water (Meyer, 2009). In 2011, the global production of GGBFS reached roughly 260-330 million tons while the slag that comes from steel production produced about 150-220 million tons (Piatak et al., 2015). In fact, the application of GGBFS as a replacement for the OPC clinker can be advantageous not only in terms of environmental concerns related to carbon dioxide reduction, raw material conservation, and industrial waste management but also from the point of mechanical, physical, and durability characteristics.

The harmful impact of humankind's activity on the natural surrounding and global warming temperature can be minimized by using GGBFS in combination with Portland cement.

For example, Crossin (2015) has reported a decrease of up to about 40% in the release of baseline greenhouse gasses thanks to the use of GGBFS as a replacement in cement. The author was sure that such an opportunity in mitigation of the harsh problem has trigged the process of credentials in eco-friendly certificates such as Singapore's BCA Green Mark, Green Building Council's Greenstar scheme in Australia, and LEED in the USA.

2.1.2 Properties

2.1.2.1 Hydration

Furthermore, the use of slag, which has a small particle size and is rich in calcium silicate hydrates (CSH), influences the rate of cement hydration showing low strength development at an early age but improved at later thanks to the secondary pozzolanic reaction (Chidiac & Panesar, 2008; Maier & Durham, 2012; C. Shi & Qian, 2000). Therefore, to improve the activity of GGBFS at an early age, different activators such as alkalis, lime, and OPC clinker may be added. As a result, during the hydration process, the slag begins a reaction generally in two phases starting from with alkalis such as Na and K at the beginning and then calcium hydroxide ($Ca(OH)_2$) later to form an additional structure of C-S-H (Özbay et al., 2016).

In fact, the process of the slag cement hydration is governed by C_2S composition that is responsible for the long-term strength rather than the C_3S phase which is the indicator of short-term development (Maier & Durham, 2012). Moreover, (Li et al., 2010) have reported that the reactivity of GGBFS is dependent on the particle size distribution. For example, if the size of the particle is more than 20 μm the reaction goes sluggish. However, the reaction in the composite cement can be finished during no more than about 24 hours if the particle size is less than 2 μm.

Since the degree of reaction depends on the fineness of slag particles, GGBFS is usually grounded smaller than OPC clinker particles in order to get better activity in cementitious properties at the initial stage. Also, depending on the types of ores and fluxing agent as well as coke impurities the activity may change with regard to the composition of the final materials. In other words, the cementitious activity of slag can be explained by the basicity index which shows the ratio of calcium oxide/siliceous oxide (CaO/SiO2) and that has to be at more than 1, with a great number indicating better activity. In short, the chemical composition of blast furnace slag primarily consists of calcium, aluminum, magnesium, and siliceous oxides (about 95% in total) and the first three magnifies the hydraulic activity but growing SiO2 reduces (Özbay et al., 2016).

2.1.2.2 Workability

Adding GGBFS into the mixture compound increases the workability of mortar and concrete. The reason for this is related to the smooth surface of particles in GGBFS and the low absorption capacity of slag, making the mixture easy to work thanks to its slippery lubricating surface (Maier & Durham, 2012). In other words, since the GGBFS particles are spherical and smaller in size than the OPC particles, the fine particles when GGBFS is added, occupy a small space between the OPC clinker particles, reducing the frictional force (Özbay et al., 2016).

2.1.2.3 Strength

Although the replacement ratio of slag with cement may vary considerably depending on the characteristics needed, it is usually considered as 50%. Slag-cement possesses pozzolanic characteristics that mean it is a reactive aluminosilicate compound (C. Shi & Qian, 2000). Pozzolans enter into a reaction with secondary products of cement hydration and increase the strength of concrete (Maier & Durham, 2012). For example, the use of GGBFS at a level of 50% and 60% have been advantageous compared to the pure OPC samples when cured in lime-water and tested at 90-d (Özbay et al., 2016). The improvement in strength caused by GGBFS is related to the fine particle size of slag and thus improved pore structure due to the consumption of $Ca(OH)_2$ and formation of CSH during the pozzolanic reaction (Chidiac & Panesar, 2008). Although slag cement is considered as a hydraulic cementitious material when utilized with OPC clinker or activated with alkali (Özbay et al., 2016), pozzolans do not have good strength properties by themselves when exposed to water (Maier & Durham, 2012). Therefore, the effect of the replacement of clinker with GGBFS on the strength characteristics of mortars and concrete is beneficial up to certain levels but adding too much will lead to the reduction in strength.

It has been reported that flexural strength can also be improved by adding GGBFS after 7-d curing thanks to changes in the pore structure, hydration products as well as compaction and density (Özbay et al., 2016). However, the authors have argued stating the results of others that 60% of replacement can be beneficial but not 40%, and 80% that leads to a decrease.

2.1.2.4 Drying shrinkage

There is not unanimous opinion in the behavior and effect of GGBFS on drying shrinkage. For instance, (Darquennes et al., 2012) have revealed that substitution of up to 50% of OPC with GGBFS demonstrated a lower degree of total shrinkage at long period than that of

OPC while the addition of more than 50% showed comparatively same level. However, (J. H. Lee & Yoon, 2015) have studied the effect of 30% and 50% replacement and reported an increase in GGBFS content caused more value of drying shrinkage than the control mixture made from pure OPC.

2.1.2.5 Porosity and durability

As discussed earlier, the substitution of cement clinker with GGBGS can improve pore structure making it dense due to the pozzolanic reaction induced by the calcium hydroxide (CH) (Maier & Durham, 2012). That, in turn, reduces the permeability of cement mixtures upon hydration.

Although there is negligible damage when the substitution does not exceed more than 50% of clinker, the freeze-thaw resistance of mortars and concretes may be damaged by adding too much slag, (Maier & Durham, 2012). Another disadvantage of using a high amount of slag in combination with OPC clinker is susceptibility at 28-day to de-icer salt scaling (Chidiac & Panesar, 2008). As indicated in the same paper, there is no obvious explanation for the bad performance but it is believed to be the slow hydration and long curing time requirement. Moreover, the resistance of slag-cement with a substitution level of 50%, 70%, and 85% to carbonation is studied and a low performance against carbonation was demonstrated by (Gruyaert et al., 2013). In other words, the carbonation rate grows with adding more GGBFS.

However, the addition of slag can be effective against alkali-silica reaction (ASR) to diminish the harmful influence of reactive aggregates in concrete (Maier & Durham, 2012). According to (Özbay et al., 2016), the replacement levels of cement with 20%, 40% and 60% of GGBFS decreased the chloride ion permeability from 2065 to 1053, 403 and 282 C, respectively.

2.2 Limestone Calcined Clay Cement (LC3)

2.2.1 Background

Despite such good properties of SCMs such as GGBFS in the replacement of Portland cement clinker, there is a barrier in the wide use of those materials. Currently, more than 80% of the materials used as a replacement for OPC clinker are only slag, limestone, and fly ash. For example, the total available resource of slag accounts for only about 5-10% of cement production (see Figure 2.2) (K. Scrivener et al., 2018). In the long term, the amount of all traditionally used SCMs such as silica fume (SF), fly ash (FA) and slag are expected to decrease due to the environmental impacts of their production.

Therefore, the use of one of the richest resources around the world, clay, is proposed as a solution for sustainable growth. Although the composition of clays may vary depending on the kaolinite content, it is more advantageous to use low or intermediate purity due to low cost in comparison with expensive high grade, usually used for the production of pure metakaolin (Martirena et al., 2018). Clays, consisting of kaolinite (at least 40%), are very pozzolanic when calcined at around 700-850ºC. It means a large amount of saving in energy consumption than that of OPC during calcination (1450ºC) (K. Scrivener et al., 2018).

In fact, the calcination of clays may be more expansive than the conventional SCMs in some locations where they are abundant. On the other hand, not all countries have a developed heavy industry that can produce the SCMs and/or cannot easily get them. Moreover, using calcined clay allows the addition of cheap limestone in high volume to reduce further the clinker content in concrete cutting down the cost of clay calcination. In this regard, a new type of cement, limestone calcined clay cement (LC3) has been invented. It is generally composed of clinker (50%), calcined clay (30%), limestone (15%), and gypsum (5%) (K. Scrivener et al., 2018).
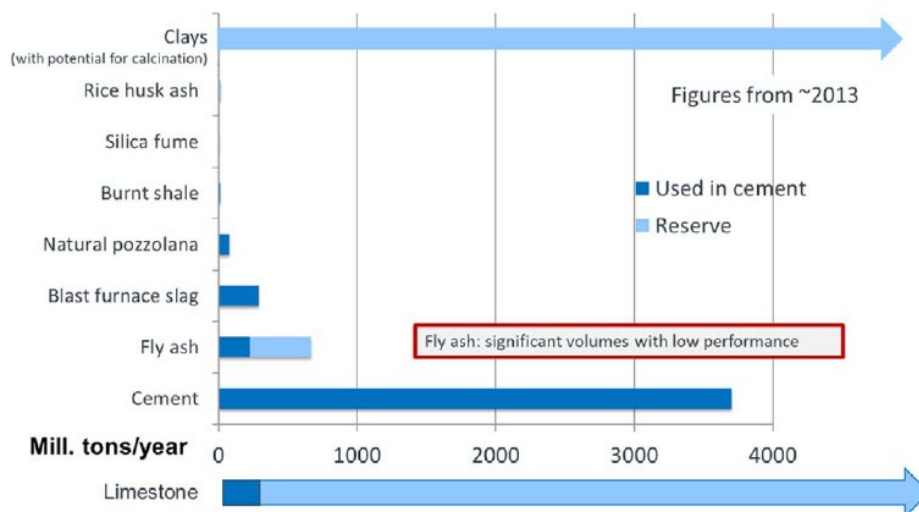
Figure 2.2: Available resources of SCMs (K. Scrivener et al., 2018).

However, it is worth being careful in the utilization of limestone since the addition of cheap and abundant limestone in a high proportion (more than 20%) requires a decrease in water to binder ratio to get corresponding concrete characteristics with regard to durability. Furthermore, the combination of limestone can trigger dilution effect but replacement of slag with a composite material of Portland limestone cement has shown to diminish it (Yuvaraj Dhandapani et al., 2018).

Utilization of LC3, on the other hand, can be beneficial regarding the environmental concerns saving about 30% of carbon dioxide release into the atmosphere in production than that of OPC. It should be mentioned that the worst case of LC3 manufacturing is more eco-friendly than the best case in OPC production with the best available technology. That efficiency is attributed to the replacement of clinker, cutting of energy use as well as electricity caused by grinding thanks to the low stiffness of LC3 composite materials (K. Scrivener et al., 2018).

2.2.2 Properties

2.2.2.1 Hydration

The phase composition of LC3 is similar to the conventional composite cement. Calcination of clays consisting of kaolinite leads to the formation of an amorphous aluminosilicate with a formula of $Al_2O_3 \cdot 2SiO_2$, also known as metakaolin. That, then, can enter into a reaction with calcium hydroxide and produce C-A-S-H structure as well as aluminate hydrates. Moreover, additional hydrate phases such as Mono- and Hemi-carbo-aluminates can be produced due to the reaction between aluminum oxide from the calcined clay and calcite from limestone forming a new phase (Antoni et al., 2012; Yuvaraj Dhandapani & Santhanam, 2017; K. Scrivener et al., 2018). According to (Y. Dhandapani et al., 2018; Yuvaraj Dhandapani & Santhanam, 2017), improvement in packing, the additional hydrates aforementioned and high reactivity of calcined clay, consuming a higher amount of Portlandite by 3 days, lead to the enhancement in filling efficiency of the compound, compact and dense microstructure due to the lower density of the phases than typical hydration products such as calcium-silicate-hydrate (SCH) and Portlandite.

2.2.2.2 Workability

The specific surface of LC3 composite caused by platelets of calcined clays leads to the high need for water upon mixing than blends made from pure OPC. Since there is a content of metakaolin, the conventional superplasticizers efficiently used in the OPC mixture can also be applied to solve the workability problem in the LC3 system (K. Scrivener et al., 2018).

2.2.2.3 Strength

Mechanical properties for the system of calcined clay, limestone, gypsum and OPC clinker has been investigated by many researchers in different combination. For example, (Maraghechi et al., 2018) have found that the compressive strength of LC3 mortar is lower

than OPC mixture at 1-d but the LC3 system has shown a comparable strength after 3-d (95% kaolinite) and even higher after 7 days of curing (≥40% kaolinite). (Yuvaraj Dhandapani et al., 2018) have studied concrete with three sets of mixtures to get compressive strength of 30 MPa (M30) and 50 MPa (M50), and common mixes (fixed w/b and binder content) made from OPC, LC3, and FA-based blended cement with a replacement level of 30% (FA30). They have reported that although LC3 contained less amount of binder it has shown higher compressive strength than FA30 but similar with OPC mixtures up to 28 days. However, the compressive strength of LC3 in common mixes has demonstrated better performance during the all-time.

(K. Scrivener et al., 2018) have published that the compressive strength of LC3 mortars consisted of clinker (50%), calcined clay (30%), limestone (15%), and gypsum (5%) is dependent on the ratio of kaolinite clay content (see Figure 2.3)
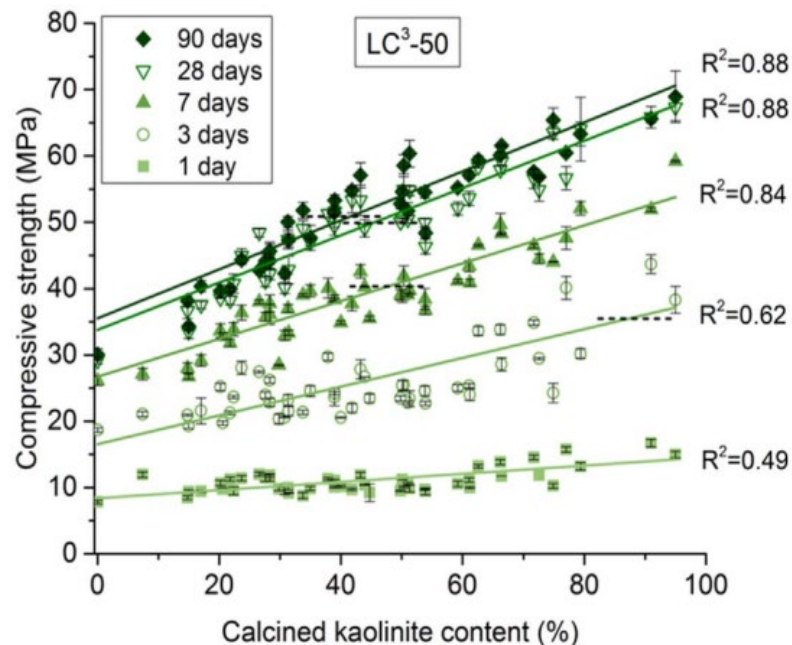
Figure 2.3: Effect of kaolinite content on the compressive strength of LC3 mortars. The dashed line demonstrates the strength of OPC mortars with gypsum and more than 90% clinker in content (K. Scrivener et al., 2018).

2.2.2.4 Drying shrinkage

Drying shrinkage is the evaporation of water out of hydration products but it should be differentiated from autogenous shrinkage which is defined by the change of relative humidity inside of concrete caused by the consumption of free water. The main factors to define the shrinkage level can be the degree of humidity, water/binder ratio, and sample dimensions

(Yuvaraj Dhandapani et al., 2018). According to the same paper, the shrinkage strain values have been comparable for LC3 and OPC after 4 weeks.

Another factor that influences the drying shrinkage is the composition of the binder. For example, growth in the level of metakaolin by three times from 5% in the binder, lead to a decrease in both autogenous and drying shrinkage development at an early age but opposite in the long term. Generally, however, the drying shrinkage is thought to decrease by the addition of metakaolin (Yuvaraj Dhandapani et al., 2018).

In the case of limestone, it varies depending on the replacement portion of limestone. Up to 10% of addition has demonstrated comparable or smaller shrinkage but more than 20% in substation caused magnification in the value of drying shrinkage. Therefore, a combination of metakaolin and limestone manifested comparable or slightly greater shrinkage (Yuvaraj Dhandapani et al., 2018).

2.2.2.5 Porosity and durability

The enhancement in pore structure can be primarily affected by many factors such as reaction kinetics, hydration rate, chemical additives, water to binder ratio, and conditions of mixture treatment (Yuvaraj Dhandapani & Santhanam, 2017). Furthermore, the pore structure characteristics of LC3 pastes may primarily depend on the initial content of kaolinite in the clay, used during calcination. For example, if the original calcined clay has kaolinite that consists of more than 65% of its composition, at 3-day a fine pore of approximately 10 nm in radius can be obtained. By increasing the curing age up to 28 days, it is possible to get a better-developed pore structure than that of OPC with a reduction of the previous number from 65% to 40%, or even lower. (K. Scrivener et al., 2018). (Yuvaraj Dhandapani & Santhanam, 2017) have reported that the volume of pores up to 1μm for mixtures made from LC3 was determined to be almost 5mm^3/g at 3-day measurement while that of OPC accounted for as high as roughly 12 times of LC3's value. Moreover, there is a linear correlation between growth in hydration products and a decrease in capillary porosity. (Yuvaraj Dhandapani et al., 2018) have published that thanks to the pozzolanic and filler effect, LC3 has shown more tortuous pores and reduced adsorption degree.

There are several studies available in the literature regarding the durability characteristics of LC3 compound such as resistance to chloride ion penetration, the performance against carbonation process, and Alkali-Sicilia reaction (ASR) (Yuvaraj Dhandapani et al., 2018; Maraghechi et al., 2018; Martirena et al., 2018; Pierkes et al., 2018; Pillai et al., 2019; K. Scrivener et al., 2018). According to (Maraghechi et al., 2018; K. Scrivener et al., 2018), the

characteristics of the LC3 system containing 50% of kaolinite in the initial calcined clay and 50% of OPC clinker has been investigated against chloride ion penetration. The results have revealed that after two years of testing, the depth of penetration accounted for no more than 10 mm for LC3 (50% kaolinite) while the cube of 40 mm was totally affected for pure OPC mixture. That is for comparison, during the accelerated test, an efficiency of 10 times in diffusion coefficient was determined for LC3 compared to OPC. In other words, as of ACI classification (FM5-578) for corrosion rate, LC3 systems is considered as negligible (>254 k.ohm-cm) based on surface resistivity against chloride ingress whereas mixtures made from OPC have from high to moderate risk (Yuvaraj Dhandapani et al., 2018).

2.3 Dielectric constant

According to performance against conductivity of electricity, there are generally two categories of materials referred to as conductors such as aluminum and copper, and dielectric materials such as most materials in road construction. Concrete is considered dielectric since it does not show any conductivity but rather can support an electrical field. In other words, the dielectric constant shows the capacity of performance of dielectric materials in storing a charge from a sender and transferring that energy (S. I. Lee & Zollinger, 2012).

One of the main purposes of utilizing the physical characteristics of cement products such as dielectric property is to track the hydration process. The dielectric property can be described by magnetic permeability and permittivity which are mainly characterized by the dielectric constant. The last, in turn, is divided into two categories. Firstly, the real part of complex permittivity or real dielectric constant. Also known as relative dielectric constant (RDC), it is defined by the relationship with vacuum dielectric constant and shows the energy amount stored in concrete. Secondly, the imaginary part is assessed by the dielectric loss (Chung et al., 2017; Shen et al., 2016; Shen & Liu, 2019).

Currently, there are a number of nondestructive examination techniques for the concrete such as maturity test, visual inspection, the pull-off resistance correlation method, and rebound hammers to evaluate or predict the concrete characteristics such as compressive strength and hydration. However, they are usually expansive, laborious, and inaccurate (Chung et al., 2017). Therefore, relatively recently a new type of non-destructive method of concrete examination has been developed based on the dielectric properties. The principle of work with a dielectric constant is generally based on the varied RDC values of different compositions in concrete. For example, the dielectric properties of water generally depend on the molecules and state of water since the unbound water in the cement-based materials has a permanent RDC of 81 (see Table

2.1) at 20°C but that is about 5 for the physically and chemically bound water due to its strong connection and difficultness in polarization. Furthermore, the other constituents of concrete such as fillers and hydration products have shown an RDC of roughly 3 to 8. Therefore, the overall dielectric properties of cement mixtures are primarily determined by the content of free water that has the largest value (manyfold) than others. That is to say that the free water is related to a water's quantity in the capillary pores and it is expected to decrease upon consumption of water in hydration process. Therefore, the content of free water determined by RDC shows the number of capillary pores and hydration degree. (Shen et al., 2016; Shen & Liu, 2019). However, the dielectric constant of cement mixtures may change upon the addition of different materials such as chemical admixtures, fibers, and SCMs (Chung et al., 2017).

Materials have also properties related to dielectric loss which can be explained by the dielectric polarization loss and conductivity loss. In other words, it shows the intensity of the waves after going through the materials. The governing factor that influences the dielectric loss is believed to be the dielectric constant and conductivity. However, the electrical conductivity is defined by the pore structure development and the solution content in it. In other words, the determination of dielectric characteristics during the hydration process can show any change in water content as well as the microstructure of mixtures (Shen et al., 2016; Shen & Liu, 2019). Any modification in pore structure during the hydration of cement mixtures such as pore-filling can affect greatly the characteristics related to the electricity (Andrade et al., 1999).

Table 2.1: Dielectric constant of materials (S. I. Lee & Zollinger, 2012).

Material	Dielectric constant	Material	Dielectric constant
Water	79-81	Clay	2-6
Limestone	4-8	Cement	3-4
Sand	3-6	HCP	4-5
Silt	4-8	Air	1

There are many ways to evaluate the dielectric characteristics of materials such as the microwave nondestructive method, the capacitance measurement, and the time domain reflectometry method. However, recently, ground penetration radar (GPR) is becoming popular thanks to its benefits related to quickness, nondestructive performance, and detection area. The principle of operation is simple as it sends a particular amount of electromagnetic energy in the form of short impulses towards specimens. These, at the reflection, are captured for the analysis via a one-dimensional electromagnetic wave propagation theory to determine the dielectric loss

through the intensity of waves measured as relative amplitude as well as the dielectric constant of concrete through the travel time (see Eq. 2.1) Any reduction in RDC and electrical conductivity causes an improvement in the relative amplitude. Moreover, any modification in the relative amplitude demonstrates the change in microstructure and small pores (Shen et al., 2016).

$$\varepsilon = \left(\frac{c}{v\,\mu}\right)^2 \qquad\qquad (2.1)$$

Where,

ε – RDC

c – speed of light in vacuum (roughly 3 x 10^8 m/s)

v – the propagation velocity of the EM impulses

µ - magnetic content, assumed as 1 due to low value of cement mixtures

The relationship between the compressive strength and dielectric characteristics such as RDC and relative amplitude can be shown (see Figure 2.4) since there is a close correlation among dielectric properties, free water content, the number of capillary pores, and compressive strength (Shen et al., 2016). (Yuvaraj Dhandapani & Santhanam, 2017) have reported that porosity can be explained by the degree of bound water since there is a correlation between growth in the level of bound water in the mixture and a decrease in porosity of cement products. It is widely accepted that the compressive strength of cement-based materials is a function of growing water to cement ratio and dielectric constant is a function of frequency and the original water to cement ratio (Chung et al., 2017).
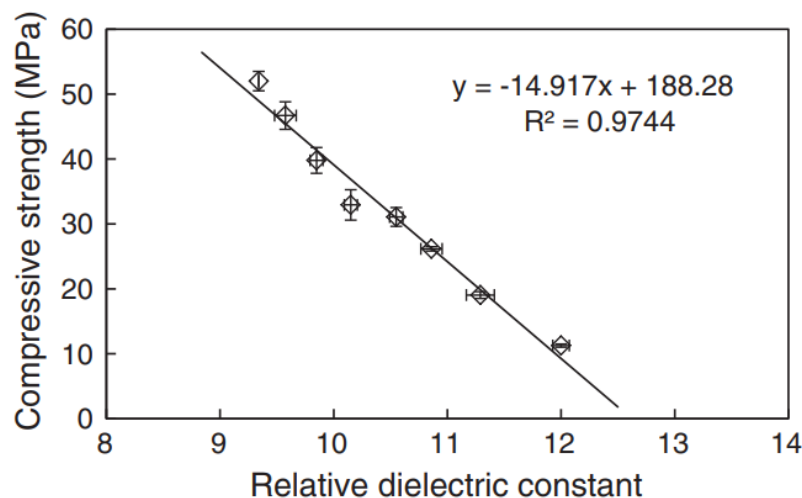
Figure 2.4:The correlation between compressive strength and relative dielectric constant (Shen et al., 2016).

2.4 Sulfate attack

2.4.1 What is "sulfate attack"?

Sulfate attack is a common way of cement mortar degradation which usually occurs in the presence of sulfate solutions in soil, seawater, and chemical plants. The mechanism of sulfate attack in Portland cement is well-known and complex depending on the content of cement and sulfate. It can manifest itself in the form of cracking, spalling, and expansion, and in some cases, in the form of softening and strength loss (Whittaker & Black, 2015). The severity of the attack is usually governed by many factors such as the permeability of cement products, concentration and types of sulfate, and the amount of tricalcium aluminate (C_3A) and calcium hydroxide ($Ca(OH)_2$) (Bescher et al., 2016; Neville, 2004).

In some cases, the different types of sulfate attacks such as thaumasite sulfate attack (TSA) may occur. It is considered different from the conventional sulfate attack due to the interaction of sulfate sources with the core structure of CSH that is the main glue of cement structures (Whittaker & Black, 2015). The formation of thaumasite requires enough source of sulfate and carbonate ions with a condition of over 10.5 in pH and low temperature and goes according to the following reaction (Skalny et al., 2002):

$$3Ca^{2+} + SiO_3^{2-} + CO_3^{2-} + SO_4^{2-} + 15H_2O \rightarrow 3CaO \cdot SiO_2 \cdot CO_2 \cdot SO_3 \cdot 15H_2O \qquad (2.2)$$
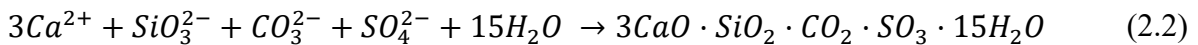
The resistance to TSA may vary depending on the types and compositions of cement blends. For example, the experiment conducted by (Ramezanianpour, 2012) has indicated that limestone cement is susceptible to TSA. Although low tricalcium aluminate cement shows poor performance, the cements free of C_3A depict no sign of TSA damage. Also, the content modification of portlandite and high sulfur trioxide/aluminum oxide ratio can be another way to control the TSA (Whittaker & Black, 2015).

2.4.2 Factors affecting sulfate attack

When comparing the test results of sulfate attack, it is vital to know what kind of factors can affect the damage degree. The beginning of the specimen expansion depends on the size of the sample and can be delayed through an increase of mortar prisms from 10x10x100mm to 70x70x280 mm, for instance (El-Hachem et al., 2012). Furthermore, the condition of curing plays a significant role in assessment. When comparing the samples cured in air and water, the first has demonstrated better resistance owing to a formed carbonation layer and consequently hindering sulfate ion transportation (Whittaker & Black, 2015).

Although both permeability and chemical resistance of composites are required to fully understand the sulfate attack expansion, permeability is a key factor to withstand against penetration of liquid and air that can contain aggressive chemicals such as chloride or sulfate ions (Khatri et al., 1997). It shows how the pores are structured in the hardened product. It is well known that OPC creates calcium-silicate hydrate (CSH) and Portlandite ($Ca(OH)_2$) along with heat when it reacts with water: (Bensted, 1983).

$$3C_3S + 6H = C_3S_2H_3 + 3CH + heat \qquad\qquad (2.3)$$

In other words, permeability explains the ratio of CSH to Portlandite (more CSH means low permeability) that directly affects the strength. The addition of GGBFS to the cement decreases the permeability because of its reaction with Portlandite to form more CSH. (Yuvaraj Dhandapani et al., 2018) has reported microstructures of OPC, OPC+30%FA, and LC3. The last has reduced its porosity at an early age. As a result, LC3 showed an excellent resistance against chloride ingress by 28 days compared to others.

Since the permeability and pore structure is defined by the amount of water, it is vital to control the water to cementitious materials ratio under 0.45 when the "safe region" can be formed if the content of tricalcium aluminate (C_3A) is below 8%. In that condition, there has not been found structure deterioration submerged in solution throughout the period of 40 years (Monteiro & Kurtis, 2003).

According to (S. Yang et al., 1996), the higher content of interfacial zones between cement paste and aggregates has accelerated the speed of sulfate attack because it has abundant hydrated crystals and high porosity which allows the sulfate ions to penetrate inside the structure. However, the resistance against sulfate attack can be increased up to 6-7-fold in case of using pretreated aggregate that contains hydraulic surface layer and inert core.

Although a high concentration of sulfate solution can hasten the damage and induce the production of gypsum it does not affect the depth of propagation in mortar specimens. Furthermore, the replacement of the using solution with a new one has been reported to slow the damage due to the smaller pH of sodium sulfate solution that interferes with the formation of ettringite and more CSH decalcification while others have argued those, stating vice versa. The true fact is that any reduction in pH of sulfate solution deteriorated the resistance of slag-added composites in the amount of below 60% against sulfate attack (Whittaker & Black, 2015).

2.4.3 Sources and mechanisms of sulfate attack

It is well known that external sulfate sources, going through the pores of the mixture, reacts with hydration products. However, the sulfate ions that penetrated into the structure require aluminum and calcium to form ettringite since it is a combination of calcium sulfoaluminate hydrate ($C_6AS_3H_{32}$). The source of aluminum can be found in the composition of CSH, hydrotalcite, and frequently AFm phases. In order to form ettringite, the AFm phases need an additional two atoms of calcium which can be taken from portlandite. In fact, ettringite is an expansive crystalline product in nature because it gains a larger volume than the products from which it is made. For example, the volume of solids can grow approximately two times from 312.7 ml/mol to 714.9 ml/mol in the case of monosulfate-ettringite and from 33.2 ml/mol to 74.2 ml/mol in the case of portlandite-gypsum. This induces internal tensile stresses in the structure which may become large enough to surpass the material's tensile strength causing cracks. However, this is not always true because some researchers claim that there is no obvious relationship between the amount of ettringite and/or gypsum formation and the level of expansion because their volume did not surpass the total capillary porosity. Therefore, a crack can happen only if ettringite forms in the confined rooms (Whittaker & Black, 2015).

Generally, there are three main types of sulfate sources that damage concrete such as calcium sulfate, sodium sulfate, and magnesium sulfate. The first one is the most straightforward and negligible attack due to possibly low solubility of calcium sulfate (1.46 g/l of SO_4^{2-}) and happens as follows depending on the C_3A content (5% or 8%) producing ettringite (Eq. 2.4). (Bescher et al., 2016; Skalny et al., 2002).

$$C_3A \xrightarrow{hydration} monosulfate\ hydrate/hydrogarnet \xrightarrow{sulfate\ attack} C_3A \cdot 3C\overline{S} \cdot 4H_{32} \quad (2.4)$$
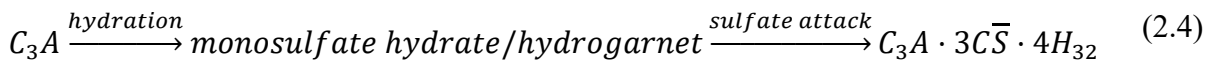
The sodium sulfate attack may involve single or multiple reactions to form ettringite. In the direct one, C_3A reacts with sodium sulfate: (Bescher et al., 2016):

$$2C_3AH_6 + 3N_2\overline{S}H_{10} \rightarrow C_3A \cdot (C\overline{S})_2 \cdot H_{32} + 2AH_3 + 6NH + 5H \quad (2.5)$$
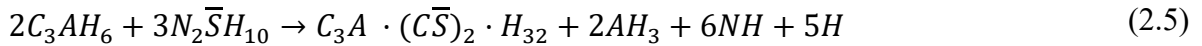
In addition, ettringite may also be produced by the two-step reaction between sodium sulfate and Portlandite which is the hydration product in Eq. 2.3. That results in the formation of gypsum which in turn reacts with sodium sulfate: (Bescher et al., 2016):

$$CH + N_2\overline{S}H_{10} \rightarrow C\overline{S}H_2 + 2NH + 8H \quad (2.6)$$

$$C_3A \cdot C\overline{S} \cdot H_{12} + 2C\overline{S}H_2 + 16H \rightarrow C_3A \cdot (C\overline{S})_3 \cdot H_{32} \qquad (2.7)$$
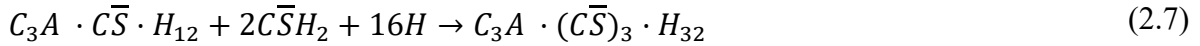
Magnesium sulfate attack is considered the most dangerous to hydrated cement products since it does not produce ettringite but rather breaks the initial CSH structure down by converting the mature cement matrix to MSH. It leads to the loss of strength since it becomes non-cementitious formation (Bescher et al., 2016). At the initial step, magnesium sulfate enters into reaction with calcium hydroxide, generating brucite (magnesium hydroxide) and gypsum:

$$CH + M\overline{S} + 2H \rightarrow C\overline{S}H_2 + MH \qquad (2.8)$$

The insoluble reaction product, brucite, will change the pH of the solution to 10.5 which is too low to stabilize CSH and ettringite and holds the process of secondary ettringite formation. The actual collapse of SCH structure starts when the content of portlandite is fully consumed because, then, the sulfate ions react with calcium silicate of core structure (Bescher et al., 2016; Whittaker & Black, 2015).

With regard to the types of mechanisms, there have been developed a few explanations such as swelling pressure, topochemical growth, and crystallization pressure. The first one is based on swelling pressure during the absorption of water by ettringite and was suggested during the work with sulfoaluminate cement containing lime and gypsum. However, this theory hardly works because of the limited capability of ettringite to absorb only 36 moles of water and to form a gel. A long time ago, the theory of topochemical growth was suggested. In contrast, now it is not believed to work due to the difference of tricalcium aluminate, AFm and ettringite in crystal structure but rather it is considered to work with a through-solution mechanism. Recently, a new explanation of ettringite precipitation has been developed. It says that a crystal is formed from solution, supersaturated with respect to the phase and the pressure is calculated according to the following equation: (Whittaker & Black, 2015).

$$\Delta P = \frac{RT}{V_m} ln \frac{IAP}{K_{s0}} \qquad (2.9)$$

ΔP - is the pressure required to stop the crystal appeared in the pore

R – molar gas constant

T – temperature (K)

V_m – molar volume

IAP – ion activity product

K_{s0} – equilibrium solubility product

$\frac{IAP}{K_{s0}}$ – the supersaturation ratio, showing a stable state when it is 1. If more than 1, the process of ettringite precipitation starts. However, if the ratio is less than 1, ettringite dissolves. The factors, affecting the crystallization pressure, are pH, humidity, pore size, and the presence of solid solutions. The practical use of the theory has lately demonstrated the amount of pressure as 21 MPa (Whittaker & Black, 2015).

2.4.4 Consequences and prevention of sulfate attack

One of the easiest ways to improve the sulfate resistance of cement mixtures is an effort in preventing the formation of expansive sulfate attack products. Generally, as a main source of ettringite, the content of tricalcium aluminate and portlandite in hydration products play a key role in securing efficient concrete structures against sulfate attack. For instance, (Monteiro & Kurtis, 2003) have reported that a lower content of tricalcium aluminate can improve the resistance.

A partial replacement of cement clinker with supplementary cementitious materials (SCMs) such as fly ash (FA), silica fume (SF), ground granulated blast furnace slag (GGBFS), and metakaolin, which contain high silica content, is another way to overcome the problems related to various sulfate attacks, including thaumasite and to reduce the formation of ettringite and gypsum (Al-Akhras, 2006; Lv et al., 2020; Whittaker & Black, 2015)

Application of GGBFS as an SCM along with OPC against sulfate attack is beneficial in many ways although the performance of such composite materials may change significantly upon the change of substitution degree. Firstly, it has no tricalcium aluminate, and adding it into cement reduces the ratio of C_3A in the blend and consumes portlandite by forming additional CSH gel (Ramezanianpour & Hooton, 2013). Also, it has been proved that a high level of slag in cement composition can improve the resistance against sulfate attack but a small amount of aluminum oxide in slag composition should be maintained. When the slag-cement hydrates, the aluminum allocates among CSH, aluminum hydrates (AFt and AFm), hydrotalcite, and the unreacted part of slag but only aluminum connected to AFm can easily enter into reaction with sulfate ions. However, most of the aluminum can be bound by CSH and hydrotalcite depending on the ratio of magnesium and aluminum, making it impossible to interact with sulfate ions. This is especially true in the case of alkali-activated systems. In other words, the sulfate attack resistance is dependent on the quantity of AFm when the replacement level is 40% and the aluminum oxide composition when the substitution is high (70%).Therefore, a high level of replacement can usually be advantageous against sulfate

attacks (Whittaker & Black, 2015). (Y. Yang et al., 2020) have calculated the volume of cracks after subjecting cement mortars with a w/c of 0.5 in sulfate solution up to 27 months. The results have shown a value of over 1300 mm^3 and less than 350 mm^3 for without and with slag, respectively. That was explained by the improvement of pore size distribution which resulted in decreased sulfate ion content in the case of slag. However, the authors believed that the mechanism of slag-cement mortar degradation is not the same as slag-free cement and happens by peeling off the surface.

Similarly, the use of calcined clay such as metakaolin and montmorillonite along with clinker has proven to be sulfate resistant thanks to their reaction with Portlandite which decreases the amount of the last to form gypsum and ettringite (Z. Shi et al., 2019). With regard to gypsum effect on sulfate resistance, Whittaker & Black (2015) have reported that a combination of gypsum with 65% slag is more sulfate resistant than 69% slag without gypsum. This can be explained by the early formation of ettringite than AFm phases prior to the appearance of sulfate ions and thus, less available aluminum to react consequently. In terms of limestone addition in cement used in the sulfate-rich environment, several papers reported no disadvantages of limestone in the level of below 10% although it can induce deterioration of structure if the replacement is higher than the indicated portion. Such poor performance by limestone against sulfate attack is explained by the enhanced water to cement ratio, thus, the compound's porosity and higher amount of sulfate ingress (Whittaker & Black, 2015).

2.4.5 Physical sulfate attack

In wet and dry cycles, sulfate attack may be shown in a different way, without any reaction between sulfate ions and hydration products but rather as precipitation of sulfate salts in the porous rooms. This phenomenon is called a physical sulfate attack. That may often happen with structures in tidal areas and/or in not fully immerged elements due to capillary action. The main source of this type of sulfate attack is sodium sulfate which can be in two forms such as thenardite ($NaSO_4$) and mirabilite ($NaSO_4 \cdot 10H_2O$). The behavior of these is mainly controlled by two conditions, namely, temperature and humidity. For example, in an environment where the temperature is lower than 32°C and relative humidity of more than 75%, thenardite is supersaturated in terms of mirabilite when the last is able to call deterioration during the precipitation. However, in the case of lower relative humidity (under 40%), thenardite can crystallize itself. (Whittaker & Black, 2015). Although it is not widely investigated the research recently done by Portland Cement Association has shown that a

physical sulfate attack is much severe than a chemical one (Zhutovsky & Douglas Hooton, 2017).

The mechanism behind this deterioration process is believed to be crystallization pressure although there are many other theories. It begins with the repetitive wetting and drying actions where the crystallization of salts occurs in a dry condition at low humidity. In fact, the real damage is caused during the dissolution of the present thenardite and conversion of the solution into a supersaturated state with respect to mirabilite (Whittaker & Black, 2015; Zhutovsky & Douglas Hooton, 2017). In other words, during the cyclic transformation of anhydrous sodium sulfate (thenardite) into dehydrate (mirabilite) high pressure might be generated that can damage the structure due to crystallization if it happens inside the pores at the edge of specimens (Neville, 2004). The deterioration can be usually seen as progressive surface scaling like in the case of freezing and thawing due to similar damage mechanisms such as crystallization & dissolution and phase transition (Zhutovsky & Douglas Hooton, 2017).

The benefits of supplementary cementitious materials are clear and well understood in chemical sulfate attack. In contrast, it is reverse in the case of physical sulfate attack since the mechanism of damage is different and SCMs make concrete mixtures even more susceptible to physical sulfate attack (Zhutovsky & Douglas Hooton, 2017). For example, CSA cement, usually known as sulfate-resistant cement, has demonstrated not better performance in wet and dry cycles (Zhang et al., 2017). Similarly, studying partially immerged samples into sulfate solution, researchers have found that cement mixtures with an addition of pozzolans such as fly ash, metakaolin, silica fume, and slags are more susceptible to physical sulfate attack than the ones without it. That, in turn, can be explained by a large number of small pores of the concrete not containing SCMs which favored the enhanced capillary suction and the surface area for drying (Whittaker & Black, 2015).

Chapter 3 – Materials and experimental program

The chapter presents basic characteristics of all materials used, a plan of the experimental program, mixed material proportions, and followed test methods.

3.1 Materials

The materials that have been used in this research are ordinary Portland cement (OPC), limestone calcined clay cement (LC3), ground granulated blast furnace slag (GGBFS), fine aggregate, superplasticizer, and water. In practice, before proportionating the compound of mixtures and mixing the aforementioned materials, these components should be analyzed in terms of basic physical and chemical characteristics. Therefore, the main properties of those constituents such as absorption capacity, specific gravity, particle size distribution, and chemical composition have been determined.

3.1.1 Aggregate properties

The quartz sand used as fine aggregate has an absorption capacity of 6.2%, a bulk specific gravity of 2.4, and fineness modulus (FM) of 1.02. The gradation of the sand used in this study for the whole mixture design can be found in Table 3.1. Prior to using the sand, it was oven-dried in order to get rid of moist content for the mix design.

The main characteristics of used sand such as absorption capacity and bulk specific gravity have been determined in the school laboratory following the procedures of (ASTM C128, 2003) and calculated with the following equations 3.1 and 3.2, respectively:

$$AC = 100 \ x \ \frac{W_{SSD} - W_{OD}}{W_{OD}} \tag{3.1}$$

$$G_{bulk} = 100 \ x \ \frac{W_{OD}}{W_{OD} - W_{sub}} \tag{3.2}$$

Where, AC – absorption capacity, %

W_{SSD} = weight of aggregate in saturated surface dry condition, g

W_{OD}= weight of aggregate in oven-dry condition, g

G_{bulk}= bulk specific gravity, measures as it is, without any manipulation, g

The purpose of identifying these characteristics is to use them in mix design. For example, bulk density is needed to calculate the exact amount of fine aggregate by weight and volume to proportionate the materials per unit volume of the mixture while absorption capacity is required to the extra addition of water to compensate the oven-dried fine aggregate's consumption during the hydration process of the specimens.

Table 3.1: Natural gradation of fine aggregate.

Sieve opening [mm]	Cum retained [%]	Percent passing [%]
0.6	0	100
0.3	17.8	82.1
0.15	76.8	5.4
0.075	4	1.4
Pan	1.4	0

3.1.2 Cementitious materials

ASTM Type I ordinary Portland cement, GGBFS, and LC3 were used to cast mortar mixture in this study. The specific gravity of these materials is 3.15, 3.05, and 2.83, respectively. The LC3 system consists of 50% cement clinker, 30% calcined clay, 15% limestone, and 5% gypsum. It has relatively coarser particles and lower CaO content than OPC. LC3 has average values of 2.89 μm (D10), 20.2 μm (D50), and 102 μm (D90) obtained from the laser diffraction method, which indicate 50% particles less than 20.2 μm and the other 50% particles are ranged between 20.2 μm and 102 μm (see Figure 3.1). The average value of D10, D50, and D90 for the GGBFS sample are 2.11 μm, 12.0 μm, and 30.3 μm, while those values for OPC are 4.03 μm, 17.7 μm, and 41.5 μm, respectively. The chemical compositions of those materials are shown in Table 3.2.Table 3.2

Table 3.2: Chemical composition of OPC, GGBFS, and LC3 (wt%).

	CaO	SiO_2	Al_2O_3	Fe_2O_3	SO_3	MgO	Na_2O	K_2O	TiO_2	MnO	Others
OPC	64.48	21.05	3.79	4.47	2.88	1.77	0.43*	-	-	-	5.73
GGBFS	59.95	22.33	4.86	1.09	2.70	3.62	0.07	0.90	2.48	1.13	0.87
LC3	60.52	16.13	7.26	6.99	5.05	0.36	0.06	0.72	1.74	0.16	1.01

*Na_2O_e – equivalent alkalis = Na_2O + 0.658 x K_2O (ASTM C150/C150M, 2020)
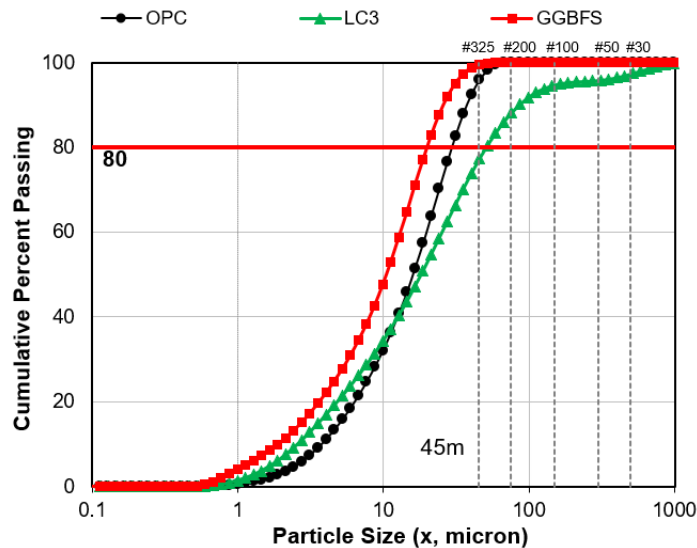
Figure 3.1: Particle size distribution of cementitious materials.

3.1.3 Superplasticizer and water

In this research, a liquid superplasticizer (SP) with a specific gravity of 1.06 has been utilized in order to maintain the proper flowability and workability of mortar mixtures. With a commercial name of MasterGlenium ACE 430 from the chemical company Basf, the superplasticizer is based on polycarboxylic ether (PCE) and has less than 0.01% of chloride ions. It corresponds to Type F and G indicated in the standard of (ASTM C494/C494M, 2013).

As the main mixing liquid, ordinary drinkable water that comes from a central plumbing system maintained at room temperature has been used for the whole set of specimens.

3.2 Experimental design

The objectives of this research are an assessment of the main properties of LC3 systems with and without the effect of adding GGBFS in the composite comparing with control samples made from OPC, with a primary focus on the durability of mortars in terms of external sulfate attack. To accomplish the aforementioned aim, a comprehensive experimental program plan has been developed which contains the following shown in Figure 3.2:

1) a detailed literature review on the previous studies about the material characteristics and sulfate attack,

2) the determination of the basic properties of the selected materials to do the mix design,

3) primary fresh and hardened properties of the mixtures related to sulfate attack,

4) analysis of the test results identifying the correlation and relationships affecting the durability of mortars and explanation of main findings.
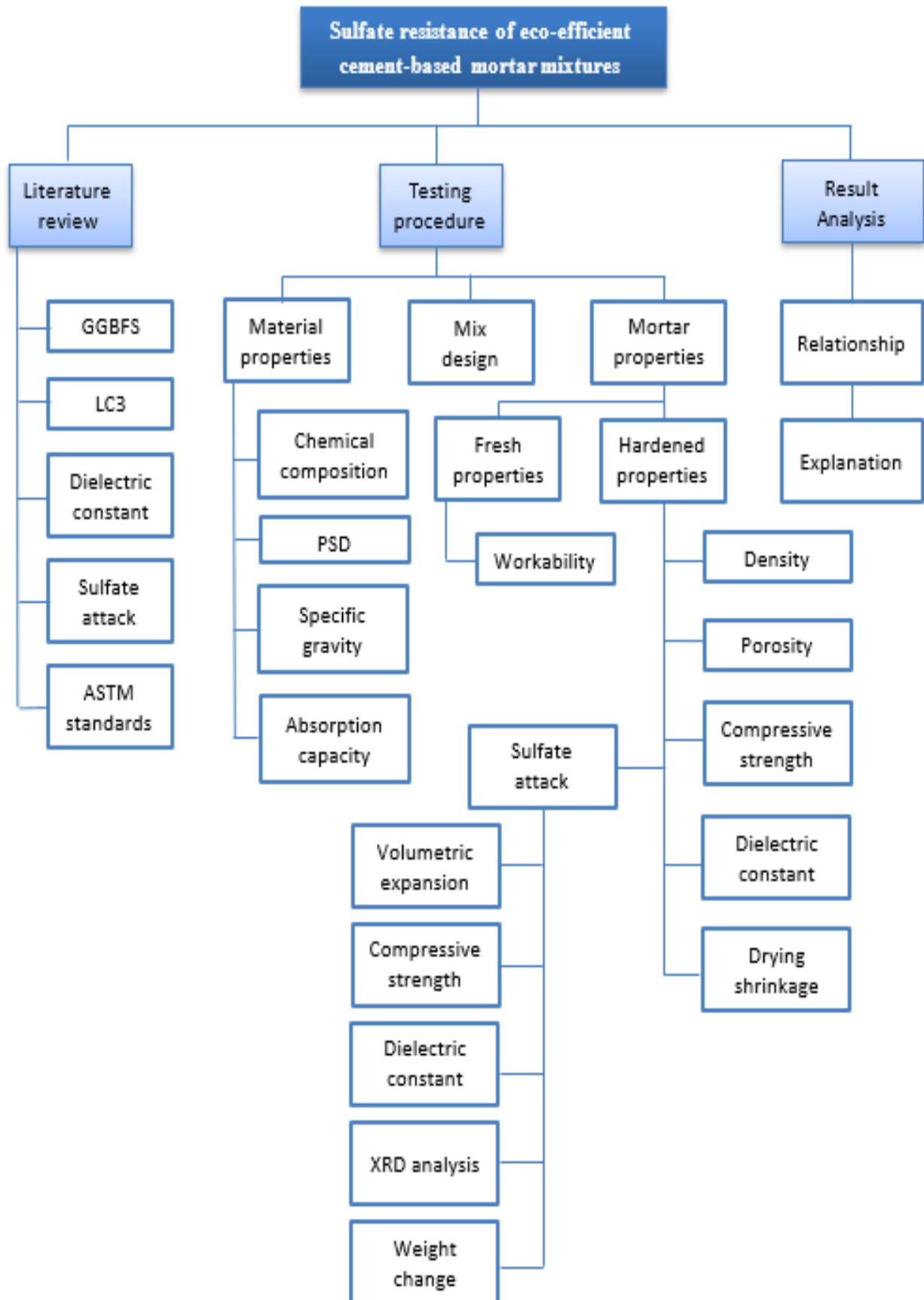
***Figure 3.2: Experimental program to evaluate the resistance of mortar mixtures
made from OPC, LC3, and GGBFS against external sulfate attack.***

3.3 Mix design

As it was written in Chapter 1 previously, the aim of this study is to investigate the performance of the eco-efficient cement called LC3 with the addition of various proportions of GGBFS and compare it with the control samples made of OPC. The primary focus of the study was the resistance of those composites against external sulfate attack Therefore, as presented in Table 3.3, a total of six mixtures such as OPC, OPC+25%GGBFS, OPC+50%GGBFS, LC3, LC3+25%GGBFS, and LC3+50%GGBFS, were prepared. The total amount of materials needed for the casting was determined by multiplying the total number of specimens by multiplying the volume of the specimen. Aggregate to binder and water to binder (w/b) ratios were fixed for all mixtures at 2.75 and 0.485, respectively. Since the LC3 contains finely ground limestone and calcined clays, a superplasticizer (SP, BASF MasterGlenium ACE 430) of 0.5% by weight of the cement was added only to the LC3 mixture to maintain the similar workability.

Table 3.3: Mixture proportion of mortars.

Mixture	Unit weight (kg/m^3)				
	OPC	LC3	GGBFS	Sand	Water
OPC	513.27			1411.49	336.45
OPC+25%GGBFS	410.17		102.54	1409.95	336.08
OPC+50%GGBFS	341.56		170.78	1408.92	335.84
LC3		504.04		1386.12	330.40
LC3+25%GGBFS		404.25	101.06	1389.62	331.23
LC3+50%GGBFS		337.45	168.72	1391.96	331.79

3.4 Curing conditions

In this study, there were mainly two conditions of sulfate attack test (see Table 3.4). Firstly, all samples were continuously normal cured in 5% sodium sulfate solution until the designed age of testing. This condition of testing was meant as a sulfate attack in this work if it was not mentioned otherwise. Secondly, the specimens underwent cycles of wetting and drying. Up to the age of 91 days, wet and dry conditions consisted of 4 days of curing in 5% Na$_2$SO$_4$ solution and 3 days of curing in air. After that, the period of wet and dry period changed to equally 7 days. Furthermore, every 77 days, the Na$_2$SO$_4$ solution was replaced with the new one.

For normal sulfate attack test at an early stage, since the compressive strength of the OPC mixture at an early age generally is higher than the LC3 mixture, additional two sets of LC3 and LC3+25%GGBFS samples were cast. The first set of LC3 and LC3 with 25% and 50% of GGBFS samples were submerged into 5% sodium sulfate solution (Na$_2$SO$_4$)

immediately after 1-day curing. The other set of LC3 and LC3+25%GGBFS specimens was exposed to 5% Na_2SO_4 solution after a 3-day saturated lime water curing. The 3-day compressive strength of the LC3 mortar mixture (6.59 MPa) was almost similar to the 1-day compressive strength of the OPC mortar mixture with 6.07 MPa (see Table 3.5).

Table 3.4: Conditions of sulfate attack test.

Mixtures	Conditions					
	1-day		3-day		Warm cured	
OPC	N-SA	W/D-SA			N-SA	W/D-SA
OPC+25%GGBFS	N-SA	W/D-SA			N-SA	W/D-SA
OPC+50%GGBFS	N-SA				N-SA	W/D-SA
LC3	N-SA		NSA	W/D-SA	N-SA	W/D-SA
LC3+25%GGBFS	N-SA		NSA	W/D-SA	N-SA	W/D-SA
LC3+50%GGBFS	N-SA				N-SA	W/D-SA

Table 3.5: Compressive strength values before the start of sulfate attack test.

Mixtures	Compressive strength (MPa)			
	1-day	3-day	6-day (warm cured)	16-day (warm cured)
OPC	6.07	11.80	15.11	
OPC+25%GGBFS	4.53	9.85	13.76	
OPC+50%GGBFS	3.57	7.75	13.43	
LC3	2.55	6.59		14.51
LC3+25%GGBFS	2.48	6.47		13.85
LC3+50%GGBFS	2.17	6.08		13.43

Moreover, to test sulfate attack resistance of mortar mixtures with high compressive strength at around 15 MPa, another set of samples was cast for all 6 mixtures. They were put in an air-tight container with saturated lime water and cured in the oven at the temperature of 45°C until the needed strength is achieved. The 16-d warm cured compressive strength of LC3 mixtures (14.51 MPA) showed a similar value with 6-d warm cured OPC (15.11 MPa) (see Table 3.5**Error! Reference source not found.**).

There are also two sets of samples with similar compressive strength for the wet and dry conditions of the sulfate attack test (see Table 3.4Table 3.4 to Table 3.5). Firstly, at low strength, 3-d cured LC3 and LC3+25%GGBFS mixtures were compared with 1-d cured OPC and

OPC+25%GGBFS samples with similar compressive strength. Similarly, as in the case of the normal sulfate attack, testing at high strength have also been conducted for the warm cured mortar mixtures.

3.5 Mixing procedure and casting specimen

The mixing of mortar mixture was carried out using a Hobart 4.7-liter mixer (see Figure 3.3) with 3-speed settings and a little modification of (ASTM C305, 2011). Testing started after a day of mixing for compressive strength and expansion. The whole procedure consists of the following steps:

1) Binding materials and water were first placed in the mixer and mixed at slow speed for 60 seconds.

2) Next, the entire quantity of sand was added to the mixer and then allowed to mix for 60 seconds at a slow speed.

3) After mixing the sand and cement with water, the mixed composite was stayed for a rest period of 1 min, including quickly scraping down into the batch any mortar that may have collected on the side of the bowl.

4) In the next step, the mixing was continued for 120 seconds until a homogeneous mortar mixture with no lumps was obtained.

Figure 3.3: Mortar mixing with a Hobart 4.7-liter mixer.

In total, 3 different types of molds with various dimensions were used for the tests indicated in the experimental program. Molds with 25x25x285 mm dimensions were cast for sulfate attack (SA) and drying shrinkage tests (see Figure 3.4). However, cubical shape molds with dimensions of 50x50x50 mm and 70x70x70 mm were cast for evaluation of compressive strength and dielectric constant (DC) of mortar mixtures, respectively (see Figure 3.4 and Figure 3.5).

In the casting process, all molds were filled with fresh mortar mixtures in two layers in order to maintain proper compaction. For example, for the compressive strength test samples, the first layer was filled approximately up to half of the molds by height and compacted manually with a wood tamper as indicated in the (ASTM C109/109M, 2016) whereas the prismatic sulfate attack and drying shrinkage specimens were performed with a steel tapping rod. After the tamping and shaking, the surface of the molds was cut from excessive material and smoothed. Upon the completion of the casting, the finished samples were covered with plastic and cured at a room temperature of 25±2°C to prevent the evaporation of water from the mixtures. 24 hours later from the mixing time, the samples were demolded and cured in the designed conditions.
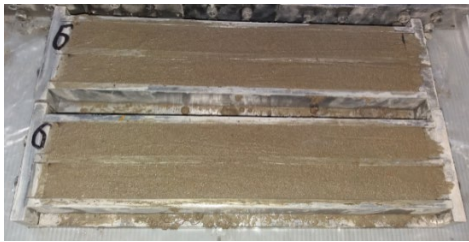
Bar samples for SA and DSH test   *Cubic samples for Compressive strength test*

Figure 3.4:Sample preparation.

Figure 3.5: Casting and smoothing the surface of the DC sample.

3.6 Test methods

3.6.1 Determination of flow of hydraulic cement mortars

Determination of flow of hydraulic cement mortars was conducted according to ASTM C 1437 (2013). The procedure is simple and consists of filling the flow mold with fresh mortar in two layers with approximately 25 mm in height each and tamping them 20 times. The tamping pressure should be just enough to ensure a homogenous filling of materials. Upon the completion of the second layer, the surface of the mold was cut off with a help of the edge side of the trowel to make it flush. Then, after cleaning the excessive materials around the mold on the table, the mold was lifted up after 60 seconds from the end of mixing. After that, 25 times of drops were performed within 15 seconds using the apparatus shown in Figure 3.6. The measurement was taken in 4 directions and an average of them was considered during the calculation of flowability as the final result as shown in Table 3.6.

Table 3.6: Flowability of mortar mixtures.

Mixtures	Flowability (%)
OPC	54
OPC+25%GGBFS	42
OPC+50%GGBFS	39
LC3	23
LC3+25%GGBFS	31
LC3+50%GGBFS	28

Figure 3.6: Apparatus for determination of flow of hydraulic cement mortar.

3.6.2 Determination of density, void ratio, and absorption

As it is well known that most durability characteristics, including sulfate attack resistance of mortars and concrete, are mainly defined by the pore structure of hydration products which can be explained by the density, free space or voids inside the sample and capacity of water absorption that is the transportation mechanism of sulfate ions. Pore structure, apart from the durability characteristics, may also have a good relationship with other hardened properties of mortar such as compressive and flexural strength.

As it is indicated in (ASTM C642, 1997), to describe the mortar sample, the parameters such as absorption after immersion (AI) (%), absorption after immersion and boiling (AIB) (%), bulk density (BD), bulk density after immersion (BDI), bulk density after immersion and boiling (BDIB), apparent density (AD) and volume of permeable pore space or voids (VV) (%) can be determined as shown in Eq. 3.3 to 3.9.

$$AI = \frac{B - A}{A} \times 100 \tag{3.3}$$

$$AIB = \frac{C - A}{A} \times 100 \tag{3.4}$$

$$BD = \frac{A}{C - D} \times \rho \tag{3.5}$$

$$BDI = \frac{B}{C - D} \times \rho \tag{3.6}$$

$$BDIB = \frac{C}{C - D} \times \rho \tag{3.7}$$

$$AD = \frac{A}{A - D} \times \rho \tag{3.8}$$

$$VV = \frac{C - A}{C - D} \times 100 \tag{3.9}$$

Where,

A = over-dry mass of specimens in air, (g)

B = surface-dry mass of specimens in air after immersion (g)

C = surface-dry mass of specimens in air after immersion and boiling (g)

D = apparent mass of specimens measured in water after immersion and boiling (g)

ρ = water density (1 g/cm^3)

3.5.4 Compressive strength test

Widely accepted that compressive strength is one of the most popular performance indexes of cement mortars to compare and evaluate their performance under different conditions. It is generally considered that the main factors to influence the strength performance of concrete are type and content of constituents, water to binder ratio that defines the density and porosity of samples, and conditions of curing. In order to control these and other factors, (ASTM C109/109M, 2016) standard test method for compressive strength of hydraulic cement mortars (using 2-in. or [50 mm] cube specimens) was followed to conduct the test.

For each testing day, which is 7, 28, 56, 91, 175 days, at least three cubical specimens with dimensions of 50x50x50 mm were cast. Before conducting the compressive strength test, density, porosity, and absorption of samples were determined to explain any difference in value. During the compressive strength test (see Figure 3.7), the same direction of tamping was kept for all samples tested to maintain consistency of the testing procedure.

Before breaking   After breaking

Figure 3.7: Compressive strength test of a sample.

3.6.3 Determination of dielectric constant

Dielectric constant values of the mortar mixtures that change over the period of time were continuously measured by using a percometer made by an Estonian company called Adek. The equipment works at the diapason of 40-50 MHz. In order to do the measurement, cubic samples with a dimension of 70x70x70 were cast for each mixture. The testing was done at the age of 1, 3, and 7 days initially, then by each week up to the 91-day period, following every two weeks after 3 months.

Before the measurement, samples cured in different conditions were pulled out from the solution, dried the surface water of the specimens, and put in the environmental chamber for an hour at the temperature of 60°C. After that, the dielectric constant values were measured on six sides of the sample with a help of a percometer (see Figure 3.8). Then, to get the average, the maximum and the minimum values were not taken into consideration to prevent bias that may have caused due to possible roughness of a bottom and a top of samples.

Figure 3.8: Determination of dielectric constant.

3.6.4 Determination of drying shrinkage

Drying shrinkage shows the degree of evaporating water from specimens by changing in length without any external forces and temperature changes. In other words, this test

evaluates the volumetric expansion or contraction of specimens. It is worth mentioning that it is different from autogenous shrinkage which is the change of humidity inside samples without considering evaporation. To determine the drying shrinkage, specimens in prismatic shape with dimensions of 25x25 mm in cross-section and 285 mm in length were used. The test was started right after the demolding of samples in one day from the start of mixing, following the American standard of (ASTM C157/C157M, 2017), "standard test method for length change of hardened hydraulic-cement mortar and concrete".

For each designed mixture, from 3 to 5 samples were cast and all samples were stored in an airtight container until the age of testing. An average of all samples was taken as the representative of a specific mixture. The drying shrinkage test was performed by reading the length change of samples with a help of a comparator based on the following formula (ASTM C157/C157M, 2017; ASTM C490/C490M, 2017):

$$L = \frac{(L_x - L_i)}{G} \times 100 \qquad\qquad (3.11)$$

Where,

L = length change of samples at a particular time, (%)

L_x = difference between the length of any sample and reference bar measured by the comparator at x time, (mm)

L_i = difference between the initial length of any sample and reference bar measured by the comparator at the initial stage, (mm)

G = nominal gauge length, (250 mm).

3.6.5 Determination of sulfate attack resistance

As a primary indictor of sulfate attack, prismatic shape samples with dimensions of 25x25x285 mm were cast for the evaluation of length change of the bar samples. After a plastic-covered 1-day air curing, all demolded specimens were fully cured in saturated lime water at a room temperature of 25±2°C until the time for sulfate attack test. The sulfate resistance test was mainly conducted according to (ASTM C1012/C1012M, 2015) "standard test method for length change of hydraulic-cement mortars exposed to a sulfate solution" but with little modification. As the goal of this study is to test the sulfate resistance of mortars at an early age, the ASTM requirement of at least 20 MPa of compressive strength before the start of the sulfate attack test was ignored. The main reason for curing the samples until they reach 20 MPa in ASTM C1012 is that it was believed the different specimens subjected to sulfate solution to have comparable

permeability resulting only in the evaluation of expansion based on the resistance of mortars to chemical attack (Khatri et al., 1997).

Measurements of volumetric expansion and weight changes of mortar bars were conducted at 1-day, 3-day, 7-day, and every week up to 91-day, then following every two weeks. The values of length change of bars were calculated according to the formula of 3.11, discussed in section 3.5.4. Furthermore, evaluation of compressive strength and change of dielectric constant values over the period of time was also measured as described in the sections of 3.5.4 and 3.5.6, respectively, for the samples submerged into 5% sodium sulfate solution in both normal and wet and dry conditions that will be discussed in the following section.

Chapter 4 – Test results and Discussion

4.1 Mechanical and physical properties

Mechanical properties of hardened mortar mixtures were assessed with respect to density, absorption capacity, and void ratio, drying shrinkage, and compressive strength throughout the period at certain ages. Moreover, physical characteristics of composites such as dielectric constant value were also determined.

4.1.1 Density/Porosity

In general, characteristics such as dry and apparent density, void ratio, and water absorption capacity describe the development of microstructure of mixtures and they are interrelated explaining any modification in a particular parameter caused by others. For example, the highest the density of specimens is the lowest the void ratio and absorption capacity are, and vice versa. These properties are considered as a key in governing durability issues such as resistance of concrete against sulfate attack. In other words, porosity and absorption capacity, thus density too, directly show the ability of sulfate ions to penetrate and transfer inside the samples of mortars which cause deleterious reactions with hydration products. Those are also important in wet and dry cycles as porosity allows to crystallization of the sulfate ions upon the drying process of samples.

The ratio of density to porosity is demonstrated in Figure 4.1 for different mixtures cured in saturated lime water measured at 7-, 28-, 56-, 91- and 175-day. In the figure, when looking at each mixture individually, there is a general trend to increase over the period and a high value indicates denser structure in the mixtures. That can be explained by the hydration of cement as time increases. Furthermore, the addition of GGBFS to both OPC and LC3 systems also demonstrates a less porous structure which is related to the fine particle size of GGBFS.

Figure 4.2 depicts the density/porosity ratio of the same mixtures submerged in 5% sodium sulfate solution after a day from mixing. It generally has exactly the same trend as the water cured samples with a clear increase of the ratio upon both time and addition of GGBFS, especially at the later age. However, if we compare each mixture in the two figures together, it becomes obvious that samples attacked by sulfate solution have a slightly higher value. This may be due to the formation of ettringite that fills the voids inside the specimens.
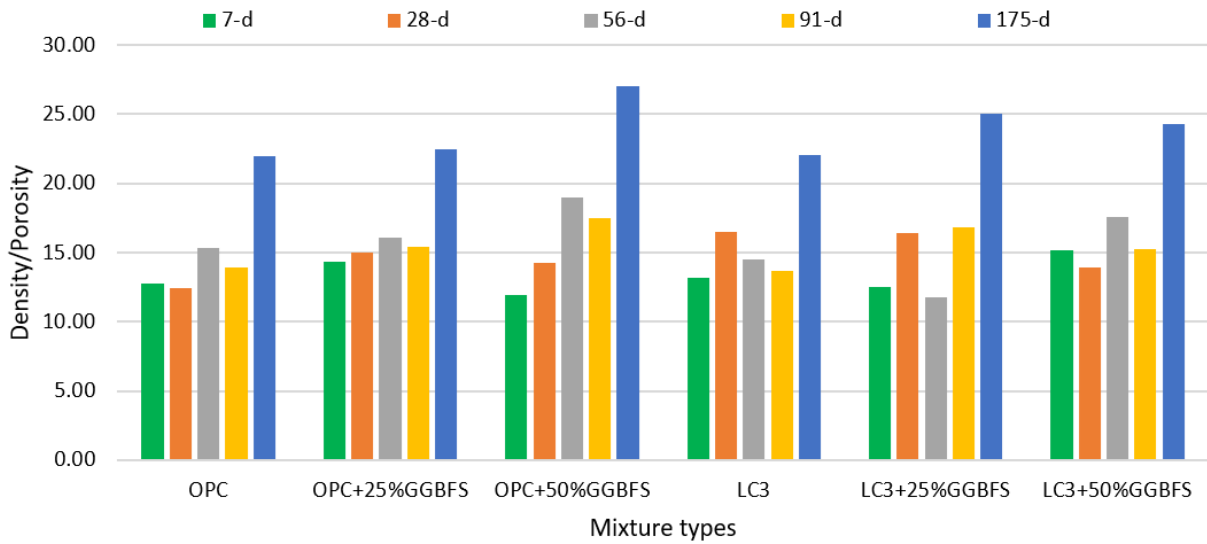
Figure 4.1: Density to porosity ratio of samples cured in saturated lime water.
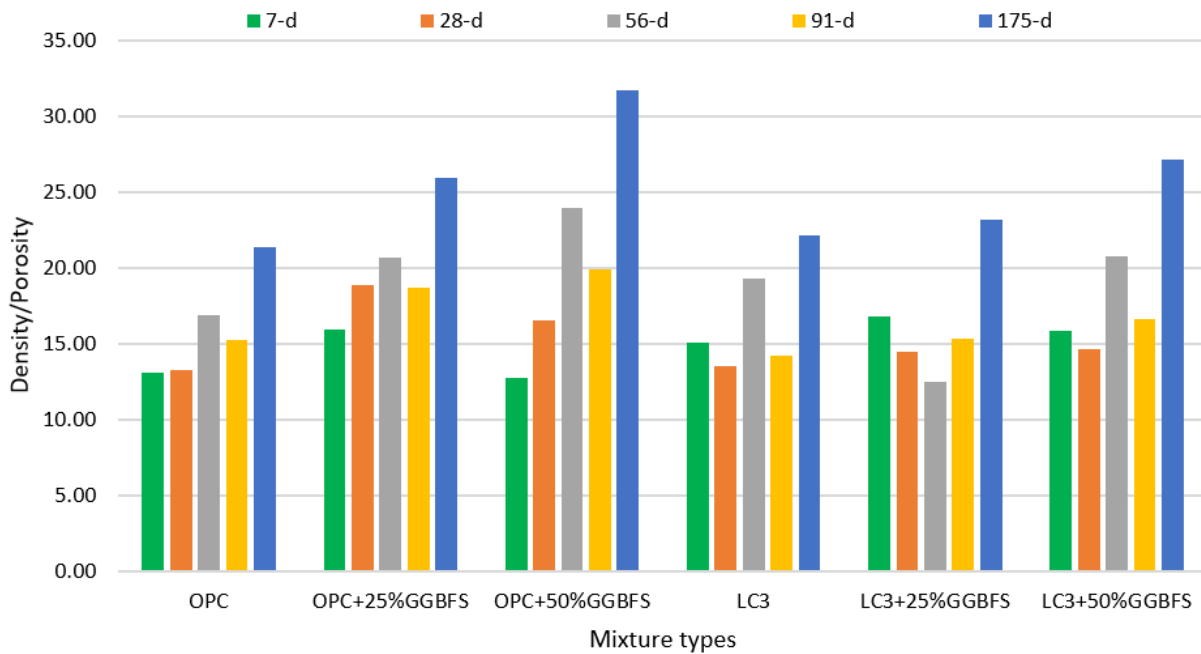

Figure 4.2: Density to porosity ratio of samples normal cured in 5% sodium sulfate solution.

In a wet-dry condition, the density/porosity ratio of samples a bit different. Although it increased over time, the addition of slag to mixtures does not affect greatly as was discussed previously in the case of normal curing. Specimens with or without GGBFS have approximately the same values (see Figure 4.3). This, as discussed in chapter 2, may be related to the poor performance of GGBFS added mixtures in wet and dry conditions if compare with normal curing. Therefore, it can be stated that the addition of GGBFS does not necessarily give a better structure in the case of wet and dry conditions.
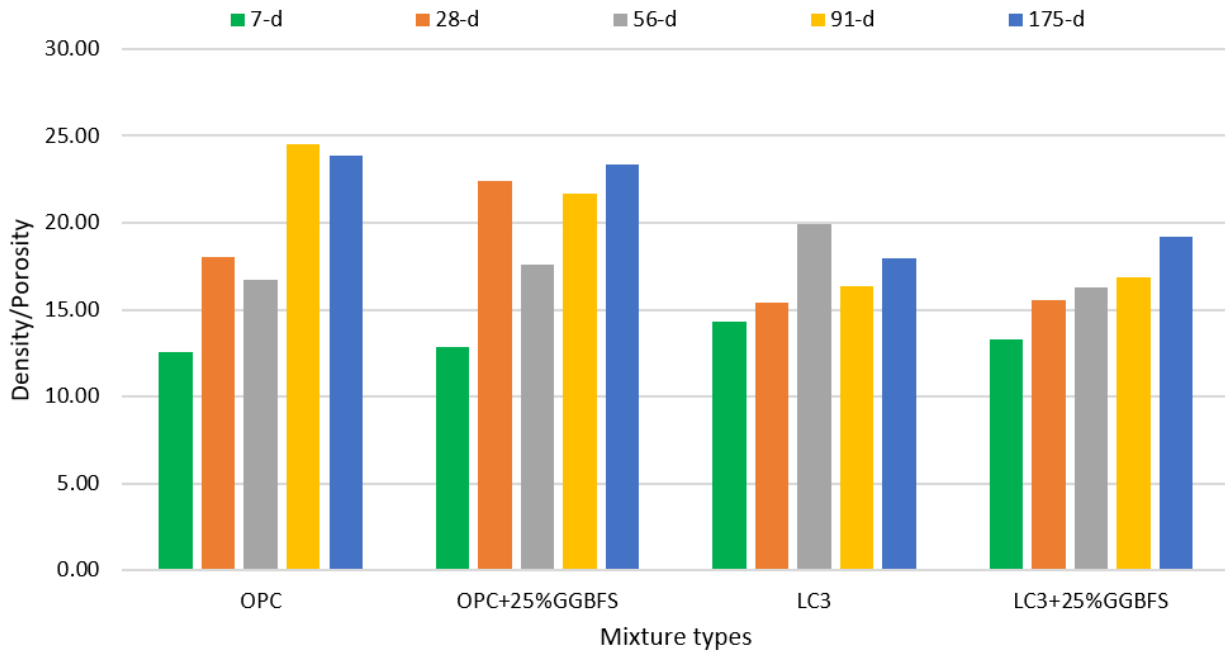
Figure 4.3: Density to porosity ratio of samples cured in the cycles of wet and dry in 5% sodium sulfate solution.

4.1.2 Drying shrinkage

One of the causes of cracks in hydration products is autogenous and drying shrinkage. The affecting parameters on the measurement of shrinkage are thought to be as w/b ratio, relative humidity, sample dimensions, and the amount of binder (Yuvaraj Dhandapani et al., 2018). Figure 4.4 illustrates the results of the drying shrinkage test that was performed right after a day from mixing for the designed six mixtures up to the age of 175-day. The length change of bars made from pure OPC and LC3 has shown similar shrinkage which agrees with the previous study of Dhandapani et al. (Yuvaraj Dhandapani et al., 2018). According to the authors, the reason behind such a comparable performance is a combination of metakaolin and limestone which have low and high drying shrinkage characteristics, respectively.

The addition of GGBFS in the amount of 25% and 50% to the OPC mixture resulted in an increase of about 46% and 39%, respectively. This supports the experiment of (J. H. Lee & Yoon, 2015) who have obtained similar results. However, several years ago, (Darquennes et al., 2012) declared that a replacement level of up to 50% GGBFS to have a smaller total shrinkage value. Interestingly, the substitution of 25% of OPC with GGBFS has slightly more shrinkage than that of 50% though the overall result was comparable. That might be explained by the governing factor of autogenous shrinkage that also demonstrated similar results in an experiment done by (J. H. Lee & Yoon, 2015) although it was reverse in drying shrinkage. However, the latter is true in the case of LC3 with a combination of 25% and 50 % GGBFS,

the level of substitution is the main factor to define the degree of drying shrinkage and agrees with the results of the study.

Furthermore, there is a good correlation with an R^2 value of at least 0.95 between drying shrinkage results and weight change of bars for all mixtures tested right a day after mixing (see Figure 4.5). This shows that drying shrinkage results from the evaporation of water which can also be explained by the linear relationship with decreasing weight change.
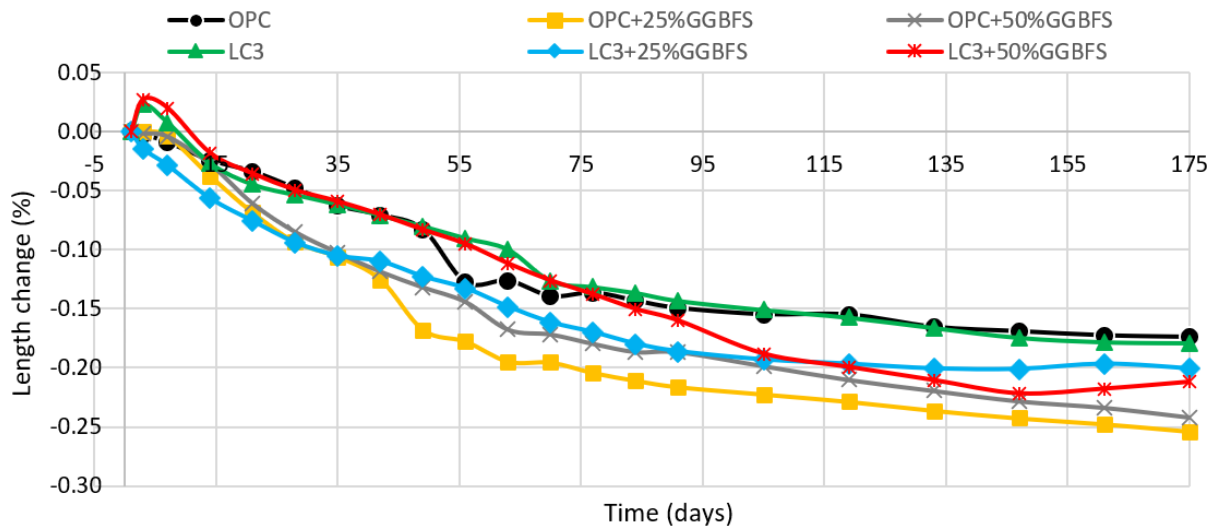

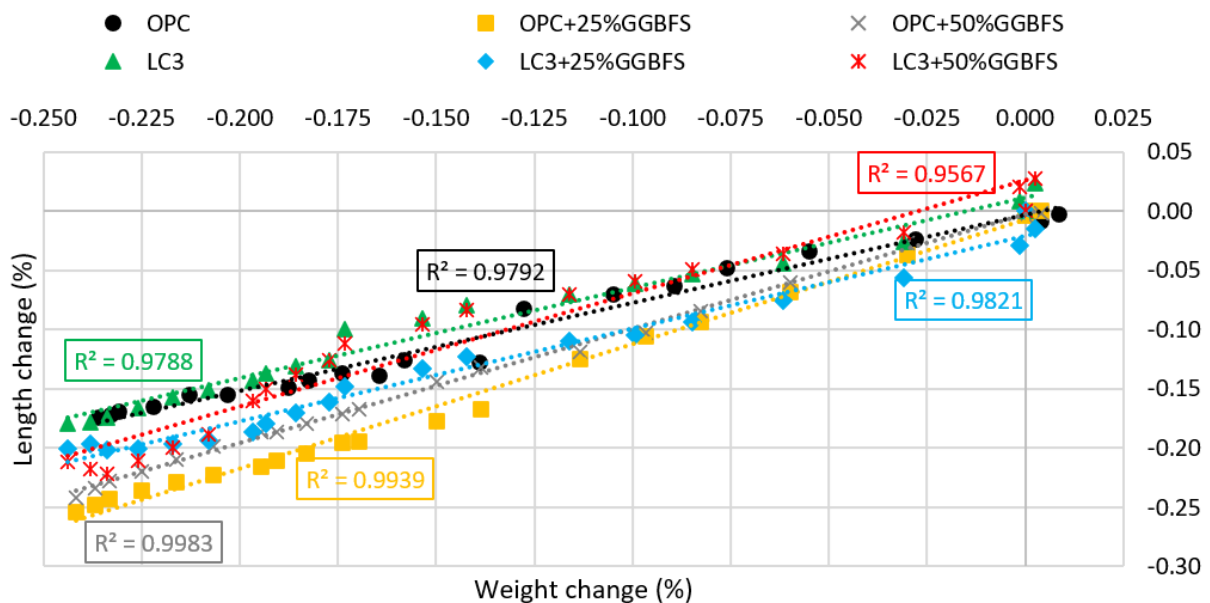*Figure 4.4: Length change of bars in drying shrinkage test.*

Figure 4.5: Correlation between drying shrinkage and weight change.

4.1.3 Dielectric constant characteristics

As early stated in Chapter 2, the main idea of the work process with a dielectric constant is based on the different values of hydration products and concrete constituents in RDC and the

content of free water inside the sample which changes over time upon the development of hydration. By knowing the level of unbound water and the degree of hydration through the determination of dielectric properties of mixtures, it is possible to correlate the quantity of capillary pores, compressive strength, and microstructure of samples (Andrade et al., 1999; Yuvaraj Dhandapani & Santhanam, 2017; Shen et al., 2016; Shen & Liu, 2019). The results of dielectric constant measurement of different mixtures cured in saturated lime water are illustrated in Figure 4.6 up to the age of 175-day. As it can be clearly seen from the figure, the overall trend for all mixtures is decreasing which shows the improving pore structure. In other words, it means that all mixtures are getting dense and less porous and supports the density to porosity data discussed early.
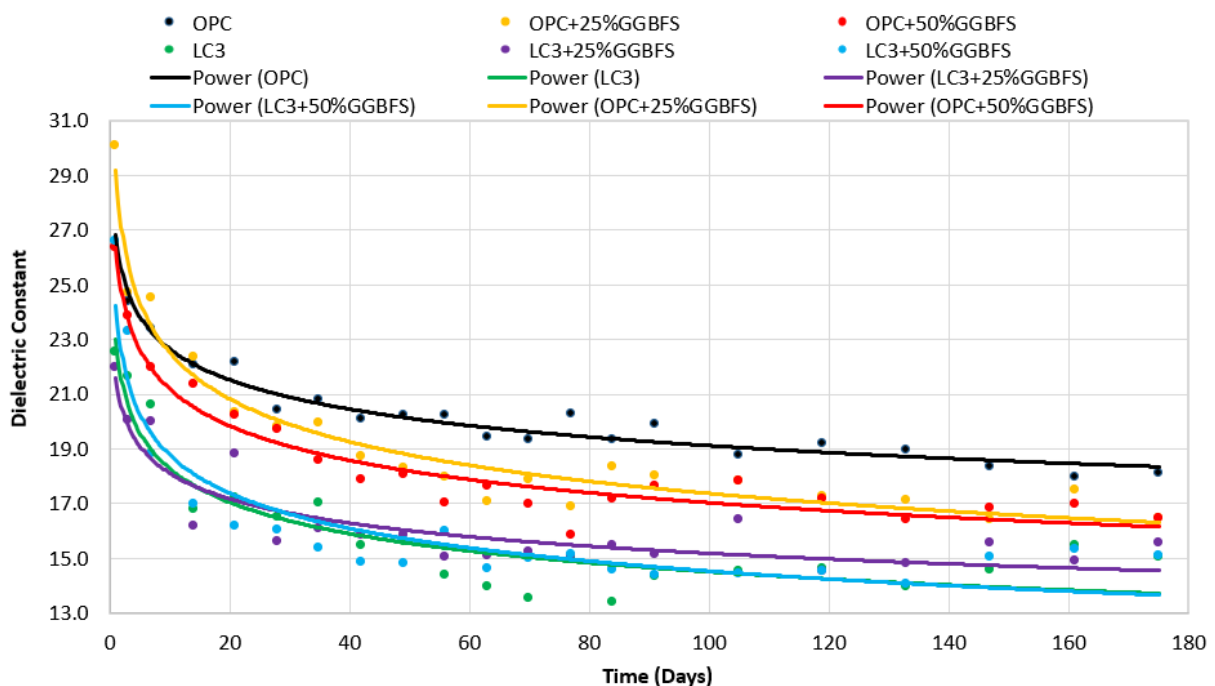

Figure 4.6: Dielectric constant values of samples cured in saturated lime water.

Comparison of LC3 and OPC shows that the first has a much lower dielectric constant value and agrees with the conclusions of (Yuvaraj Dhandapani & Santhanam, 2017) who also obtained similar results. According to the same paper, that may be attributed to the high reactivity of calcined clay that consumes water and portlandite forming additional aluminum hydrates and improvement in packing that results in better filling and denser microstructure. The effect of adding GGBFS to OPC can also be seen as it improves the structure of samples making it denser than a pure OPC mixture. However, in the case of LC3, the combination of GGBFS with cement has demonstrated comparable results.

The results of blends during sulfate attack, however, exposed to 5% sodium sulfate solution with a low initial strength showed a higher value of a dielectric constant by the age of 175-day for LC3 contained composites than the ones with OPC (see Figure 4.7). Furthermore, a comparison of dielectric constant values in water cured and sulfate attack reveals that the last saw a larger number. These might be explained by the formation of ettringite absorbing more water inside the specimens that has a chemical formula of $Ca_6Al_2(SO_4)_3(OH)_{12}26H_2O$. In other words, these 26 molecules of water increase the content of present water, thus dielectric constant in the sample. These results can be verified by expansion and XRD characteristics of mixtures which will be discussed later.
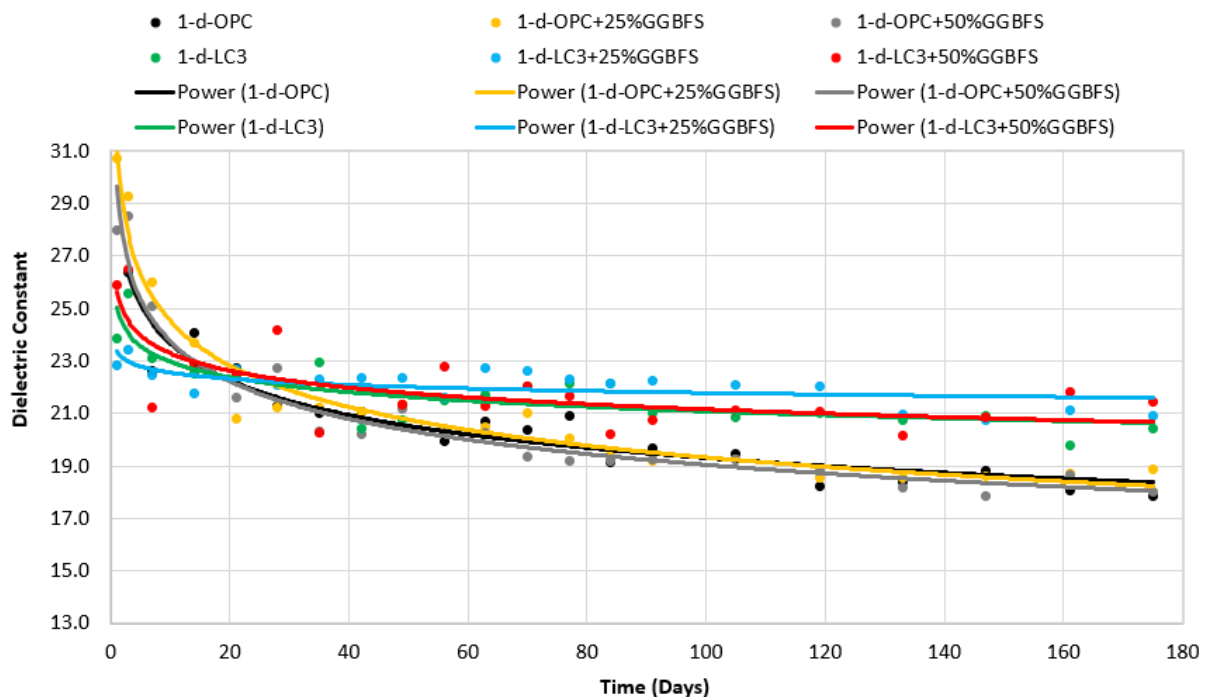

Figure 4.7: Dielectric constant values of composites subjected to 5% sodium sulfate solution after 1-d from mixing.

4.1.4 Compressive strength characteristics

4.1.4.1 Effect of curing environment and addition of GGBFS on compressive strength

Compressive strength development of mixtures at two different curing conditions (cured in lime-saturated water and exposed to 5% Na2SO4 solution) is presented in Figure 4.8 to Figure 4.9. The compressive strength of OPC mixtures with/without GGBFS is roughly 1.5 times higher than that of LC3 mixtures, regardless of curing age and curing condition. The addition of GGBFS to the OPC or LC3 mixture led to an increase in compressive strength irrespective

of the curing age. These results may be attributed to the pore refinement effect of GGBFS material which has a finer particle size than OPC and LC3 as shown in Figure 3.1.
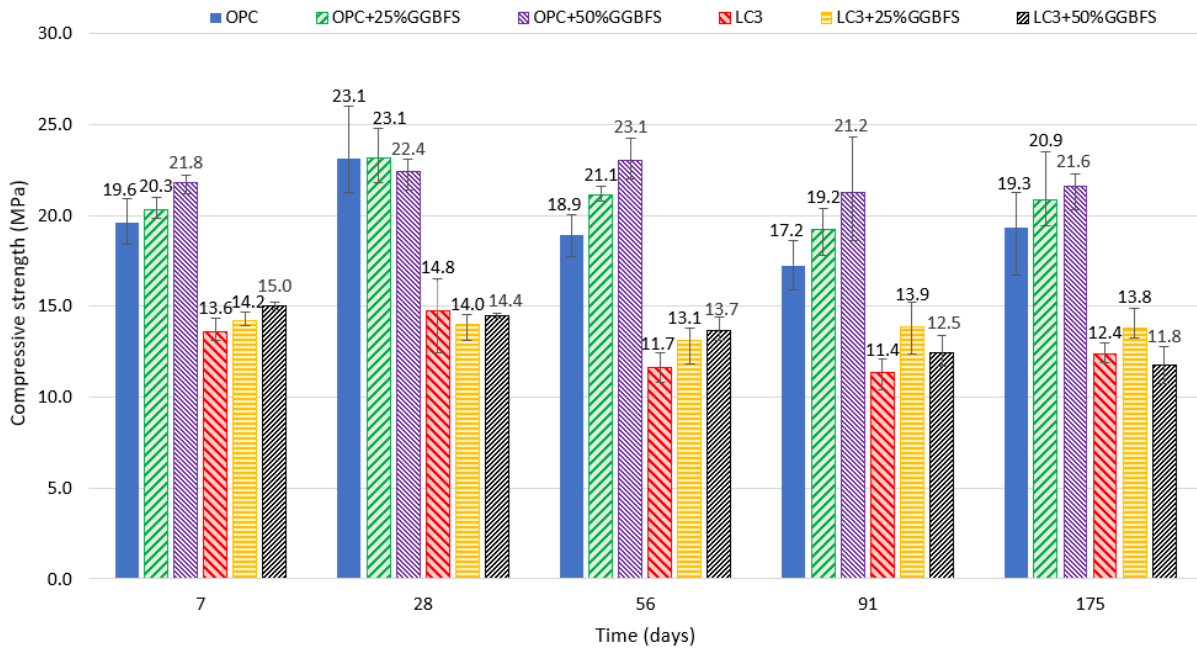

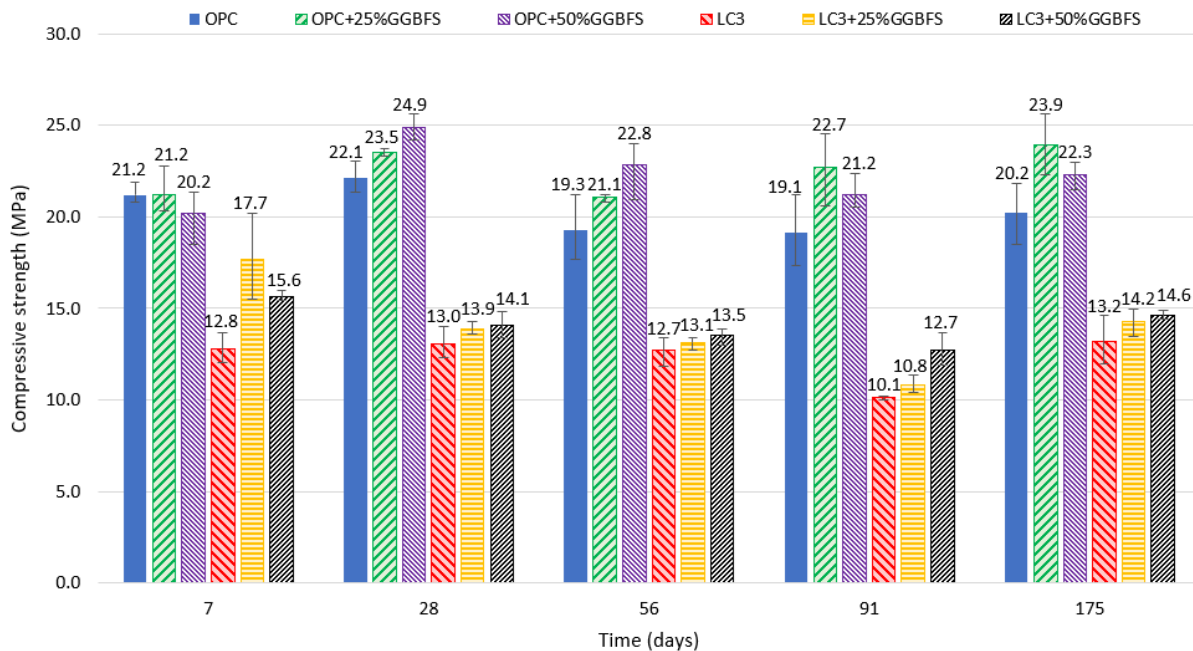*Figure 4.8: Compressive strength of mixtures cured in lime-saturated water.*

Figure 4.9: Compressive strength of mixtures cured in 5% sodium sulfate solution.

Figure 4.8 to Figure 4.9 also show that mixtures exposed to Na_2SO_4 solution have higher compressive strength than water-cured mixtures irrespective of cement type and the incorporation of GGBFS. This result is agreed with the previous research (Tian & Han, 2017). In an early sulfate attack period, the pore structure of the mixture is filled with sulfate attack

products (e.g., ettringite and gypsum) due to the chemical reaction between tricalcium aluminate (C_3A) and sodium sulfate (Na_2SO_4) (see Figure 4.10). This increases the mixture's mass, consequently increasing compressive strength

4.1.4.2 Effect of wet-dry cycling on compressive strength

The effect of wet-dry curing is totally different from normal curing. In other words, apart from the chemical reaction between sulfate and hydration products, there may also be the process of sulfate salt crystallization in the case of wetting and drying, also known as physical sulfate attack. The result of the compressive strength test is illustrated in Figure 4.11. The test was conducted based on similar initial pre-sulfate attack strength of samples and then cured in 5% sodium sulfate solution with altering wet and dry cycles. The huge difference clearly seen at the first glance in comparison with a normal sulfate attack is the effect of adding GGBFS. In other words, the combination of GGBFS with cement showed a reverse result in the wet-dry condition. This may be attributed to a large number of small pores in the mixtures without GGBFS that benefit from better capillary suction and surface area for drying (Whittaker & Black, 2015).

E-ettringite, F-ferrogedrite, G-gaylussite, P-Portlandite, A-augelite, Q-quartz, Cr-cristobalite, SS-sodium silicate, M-mirabilite, Gi-gismondine, CSH-calcium silicate hydrate, H-hydrocalumite, CS-calcium silicate, As-astrophyllite, Au-augelite, St-sturmanite, C-calcite, CO-calcium oxide
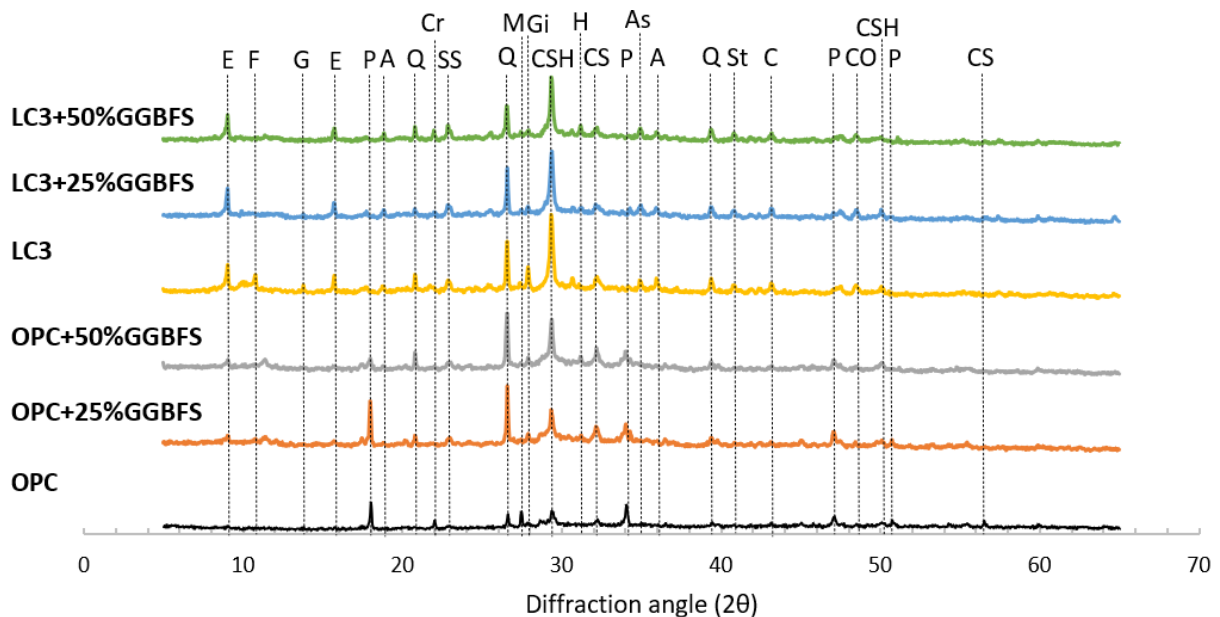

Figure 4.10: XRD results of compressive strength samples exposed to 5% sodium sulfate solution with initial low strength at 175-d.
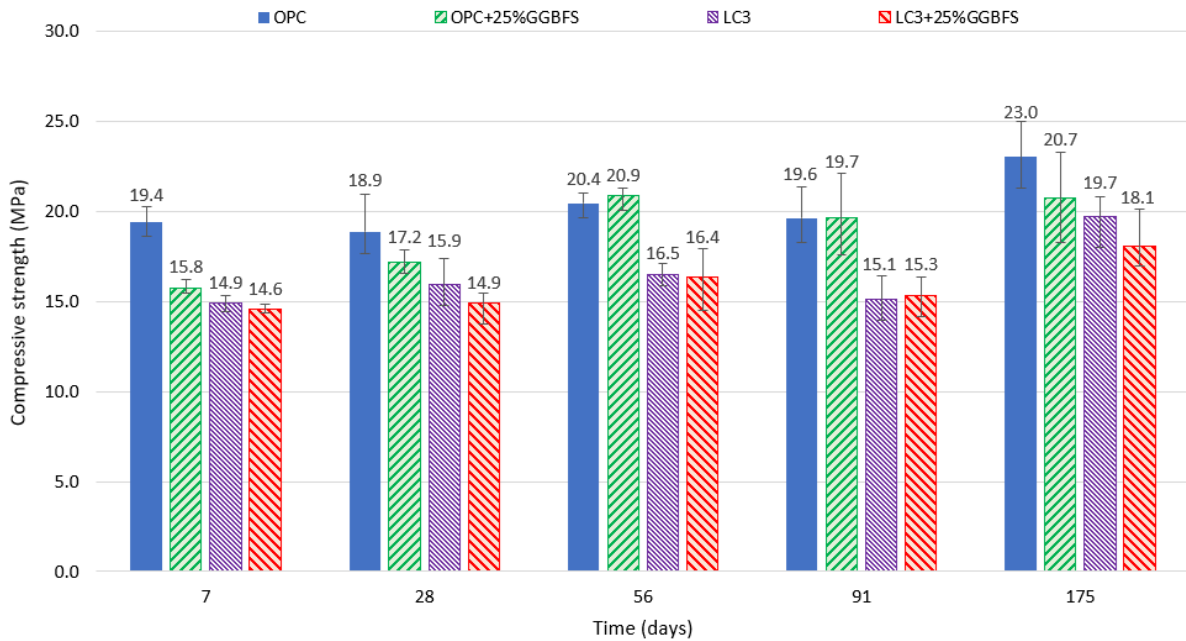
Figure 4.11: Effect of the wet and dry cycle on the compressive strength of mixtures.

If to look at the overall trend, the strength of each mixture has increased over the period of time in wet and dry condition. In addition, there is an increase in strength compared to a normal sulfate attack although cracks can be found on the edge of all mixture samples in a wet-dry condition at the age of 175-day after 18 cycles (see Figure 4.12). The rise might be caused by the formation of sulfate attack reactions (see Figure 4.13) and precipitation of sulfate salts which make the specimens denser. The appearance of cracks is explained by (Neville, 2004) due to the generation of high pressure upon the cyclic transformation of the anhydrous sodium sulfate into dehydrate that damages the sample structure during the crystallization which takes place inside the pores at the edge of samples.
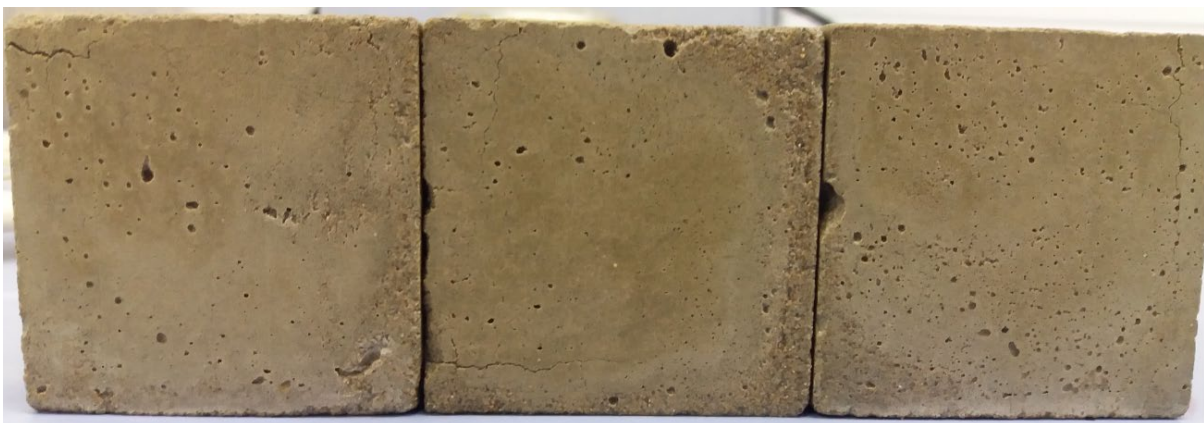

Figure 4.12: Cracks (similar to all mixtures) appeared in W/D condition at 175-d for samples with low initial strength.

E-ettringite, G-gypsum, M-magnesiocarpholite, P-Portlandite, A-augelite, Po-potassiumalum, Q-quartz, Gi-gismondine, CSH-calcium silicate hydrate, CS-calcium silicate, As-astrophyllite, St-sturmanite, C-calcite, Co-calcium oxide,
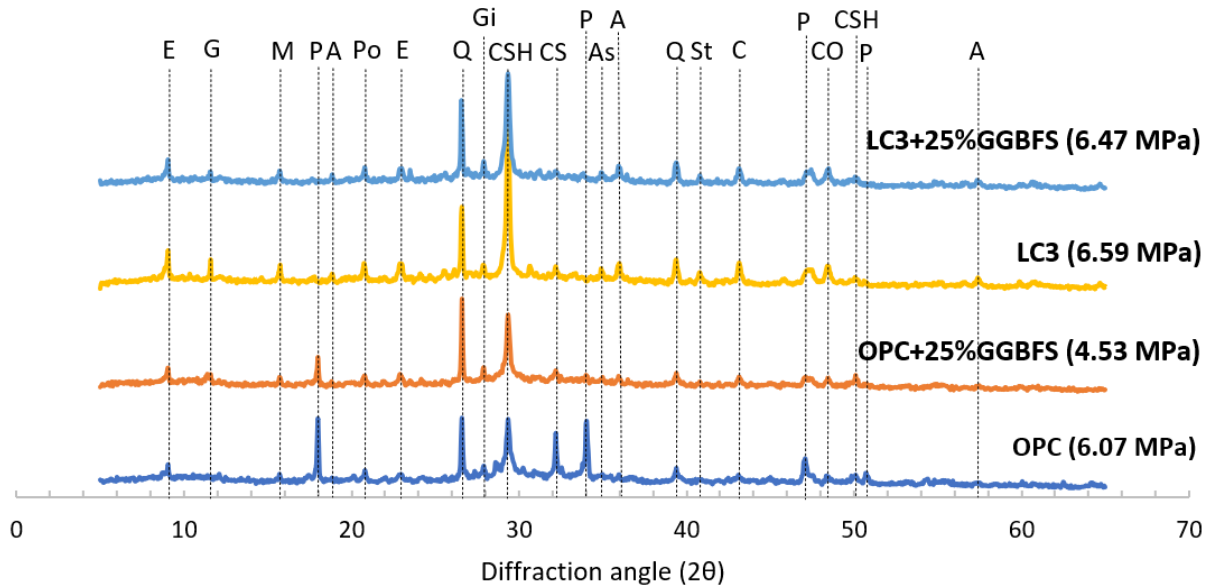

Figure 4.13: XRD results of W/D mixtures submerged in sodium sulfate solution at an early age.

4.2 Sulfate attack resistance

4.2.1 Effect of curing age on sulfate attack resistance

Figure 4.14 illustrates the expansion characteristics of mixtures submersed in Na_2SO_4 solution by measuring the length change of mortar bars. Measurements were conducted every week until 91 days and then followed by every 2-week interval. As expected, LC3 mixtures that had lower compressive strength (only 1-day curing) present higher expansion forming more ettringite than other mixtures regardless of adding GGBFS which can be verified by XRD results in Figure 4.10. This result may be explained by the percentage of density to porosity ratio (D/P). While the 1-day cured LC3 mixture has 12.7% of D/P, OPC and OPC+25% GGBFS mixtures have 12.9% and 13.0% of D/P, respectively. The lower percentage of D/P indicates less densified and poor microstructure that can be subjected to more Na_2SO_4 solution. It should be noted that the 3-day cured LC3 mixture has 12.8% of D/P that is lower than OPC and OPC+25%GGBFS.

Nevertheless, a 3-day cured LC3 mixture (6.59 MPa) with a similar compressive strength with OPC showed an opposite trend. The expansion of this mixture is about two times lower than that of OPC by 175-day. Interestingly, on the other hand, the addition of 25%

GGBFS experienced a comparable expansion for both types of cement provided that they have a similar initial compressive strength. When the replacement level was increased to 50%, the resistance of mixtures was further improved for both types of cement.
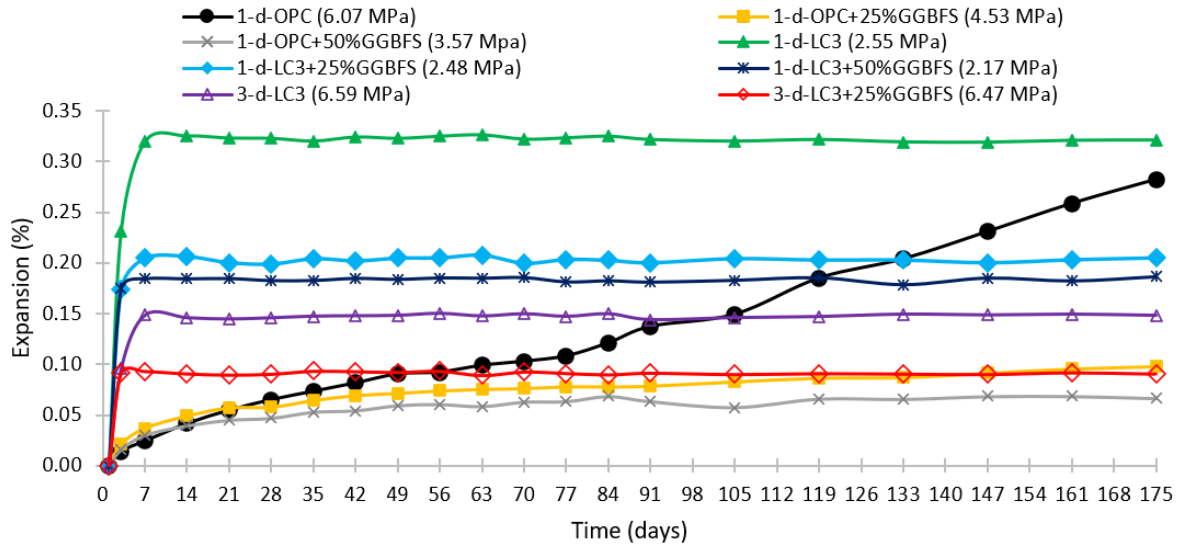

Figure 4.14:Expansion characteristics of mixtures exposed in 5% Na₂SO₄ solution at an early age.

Interestingly, all LC3 mixtures regardless of containing GGBFS had a significant expansion up to 7-day, and then they showed a negligible expansion (plateau) throughout the measurement period. This may be attributed to the following: in the LC3 mixture, calcium carbonate in limestone reacts with alumina from the calcined clay, forming supplementary aluminate ferrite monosulfate (AFm) phase, calcium aluminum silicate hydrate (C-A-S-H), and stabilizing ettringite. Antoni et al. [7] reported that "ettringite increases with time in the LC3 mixture but seems to level off around 7 days". Furthermore, studying the critical pore size development and electrical properties of LC3 mixture, (Yuvaraj Dhandapani & Santhanam, 2017) have concluded that LC3 obtains better pore structure by the age of 7 days. As expected, the OPC mixture with a higher D/P showed a lower expansion initially, and its expansion was below 0.1% up to 70 days. The expansion of the OPC mixture gradually increased and then exceeded that of the LC3 mixture at 105-day, showing approximately twice as high as the LC3 expansion at 175-day.

In the case of mixtures subjected to sulfate attack with initial high compressive strength, a trend in expansion for the samples made from LC3 is totally different from the tests based on low initial strength. In order to get a similar initial high strength at around 13-15 MPa that

results in comparable pore development for all mixtures before the sulfate attack, all samples were cured in saturated lime water in the oven at 45°C. The 16-d warm cured LC3 systems showed a comparable strength with OPC cured for 6 days. The results of sulfate attack on these samples with their compressive strength at the beginning of the test are demonstrated in Figure 4.15.

The expansion characteristics of the LC3 and the LC3+25%GGBS mixture experienced only a negligible value of fluctuation at around 0 to 0.01%. However, interestingly, the LC3+50%GGBFS mixture showed a slight shrinkage of 0.01%, indicating the insignificant effect of sodium sulfate on it. Such a better performance, in comparison with low-strength specimens, is explained by the denser structure of samples that have a density/porosity value of 16.25% and 16.45% for LC3 and LC3+25%GGBFS, respectively. In other words, as discussed in the previous paragraph, LC3 systems develop a good pore structure by the age of 7-day, while it is in the saturated lime water during 16-day curing, that prevents penetration of a large amount of sulfate ion. Furthermore, upon 16 days, the LC3 system generates enough supplementary aluminate ferrite monosulfate (AFm) phase and calcium aluminum silicate hydrate (C-A-S-H) that stabilizes the formation of ettringite.
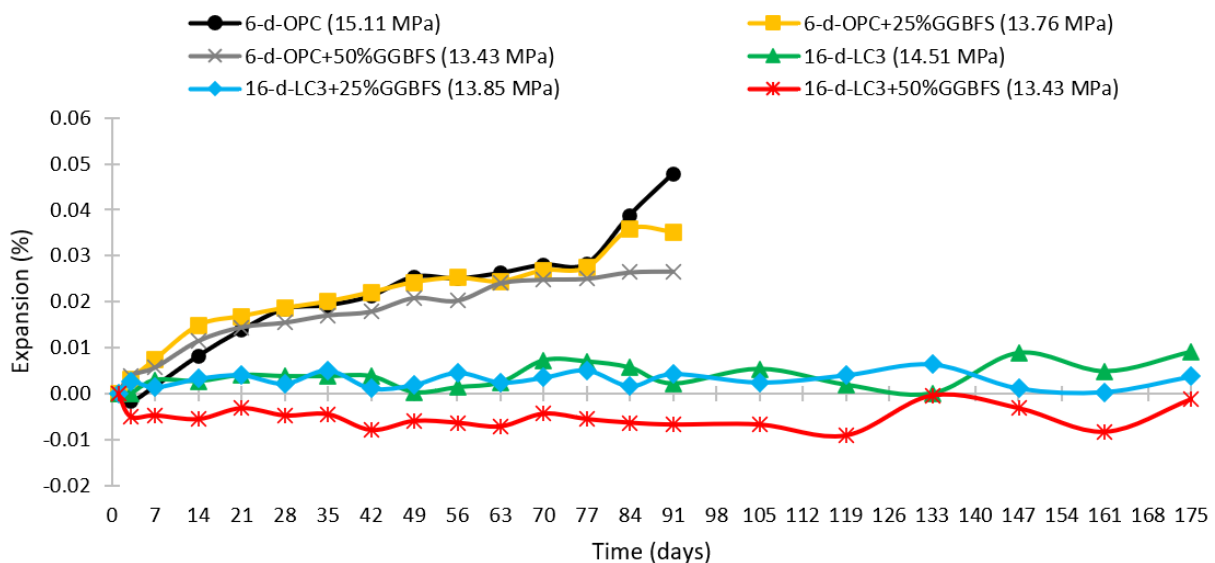

Figure 4.15: Expansion characteristics of warm cured mixtures with initial high strength exposed in 5% Na2SO4 solution.

The mixtures made from OPC, on the other hand, demonstrated a steady increase in expansion although the value for all samples was under 0.05% at the age of 91-day. Such a good performance of more than two times compared to low strength samples is probably related to the evolution of pore structure. For example, the ratio of density to porosity in percent for

OPC, OPC+25%GGBFS, and OPC+50%GGBFS mixtures upon the start of sulfate attack is 13.79%, 14.32, and 16.0%, respectively. These numbers are much higher than that of 1-d cured samples. Furthermore, a replacement of OPC with GGBFS did not show any considerable difference up to 77-day. In contrast, by 91-day, the importance of adding GGBFS comes into the picture, decreasing slightly the degree of expansion. That, as already discussed earlier, might be attributed to the refinement of pore structure thanks to a small particle size of GGBFS and pozzolanic reaction.

4.2.2 Effect of supplementary cementitious materials (SCMs) on sulfate attack resistance

Figure 4.16 shows the expansion behavior of mortar mixtures with and without containing 25% and 50% GGBFS at 28-, 56-, 91-, 133- and 175-day. Mortar mixtures containing GGBFS resulted in lower expansion at all ages irrespective of cement type and initial strength (curing period). This improvement may be due to the pozzolanic reaction of GGBFS, which consumes portlandite ($Ca(OH)_2$) which is the primary source of calcium ions to form ettringite and gypsum (Z. Shi et al., 2019). Furthermore, a partial replacement of clinker with GGBFS reduces the amount of C_3A in the composite cements since GGBFS has no or low tricalcium aluminate (Ramezanianpour & Hooton, 2013). This is clearly seen in the replacement level which becomes better by increasing the amount from 25% to 50% in both types of cement. The combination of GGBFS also results in the evolution of pore size distribution hindering penetration of sulfate ions (Y. Yang et al., 2020) which can be proved by the results of absorption capacity at the age of 175-d. For example, the pure OPC mixture had an absorption capacity of 5.27% but 25% and 50% GGBFS addition reduced it to 4.24% and 3.39%, respectively.

The reduction percentage in the expansion of mortar mixtures due to sulfate attack was calculated using Eq. 4.1.

$$R_{exp}(\%) = \frac{(\varepsilon_{without\ GGBFS} - \varepsilon_{GGBFS})}{\varepsilon_{without\ GGBFS}} \; x \; 100 \qquad (4.1)$$

where, R_{exp} = a reduction percentage in expansion of the mortar bar, $\varepsilon_{without\ GGBFS}$ = expansion of mortar bar without GGBFS, and ε_{GGBFS} = expansion of the mortar bar containing GGBFS.
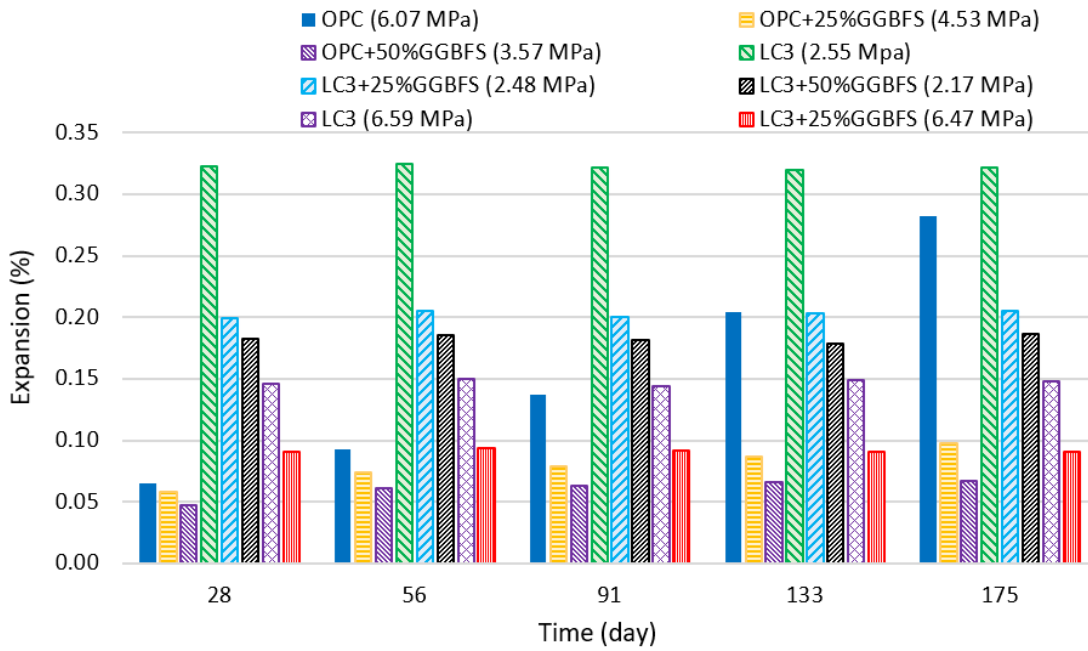
a) Expansion characteristics
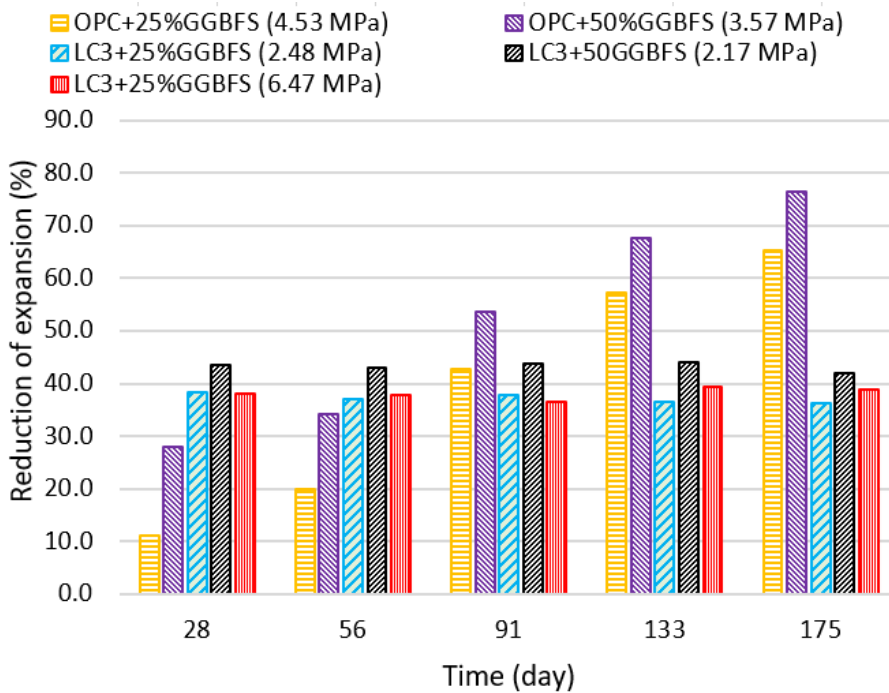
b) Reduction of sulfate attack expansion

Figure 4.16: Effect of GGBFS on sulfate attack expansion.

The effect of GGBFS on the reduction of sulfate attack expansion is presented in Figure 4.16 (b). The reduction of OPC mixture in expansion at 25% and 50% replacement with GGBFS increased over time. For example, the R_{exp} at 28 days was 11.2% and 28.0% while R_{exp} at 175

days was 65.3% and 76.4%, respectively. Because the OPC mixture gradually deteriorates over time, GGBFS in the OPC mixture is more efficient to reduce the sulfate attack expansion. For the LC3 mixture, the GGBFS is more effective in reducing the expansion of the mixture at an early age (about 40%) in comparison with OPC but over time the change becomes the opposite. As shown in Figure 4.16, the expansion of the LC3 mixture occurs at an early age (up to 7-day) regardless of the initial compressive strength, and then it stops. The replacement level of LC3 with 25% GGBFS on expansion at low and high strength does not differ greatly although it becomes slightly better at higher strength. The combined use of LC3 and GGBFS seems to provide a synergistic effect on reducing the expansion due to sulfate attack.

4.2.3 Effect of wet-dry cycling on sulfate attack resistance

It was said that wet and dry cycles can change the degree of damage caused by external sulfate attacks to mortars and concrete. Length change measurement of OPC and LC3 mortar mixture bars with and without the addition of 25% GGBFS exposed to sulfate solution at low strength is presented in Figure 4.17. Initially, up to the age of 56-day, mixtures made from OPC does not show any expansion and stayed near zero. However, after that which corresponds to 7-8 cycles of wet-dry, they begin a continuous increase in the expansion that reached 0.38% and 0.58% at 175-day for OPC and OPC+25%GGBFS, respectively. It is worth mentioning that the addition of GGBFS to OPC resulted in greater expansion almost all the ages reaching its peak of about 1.5 times in the difference at 175-day.
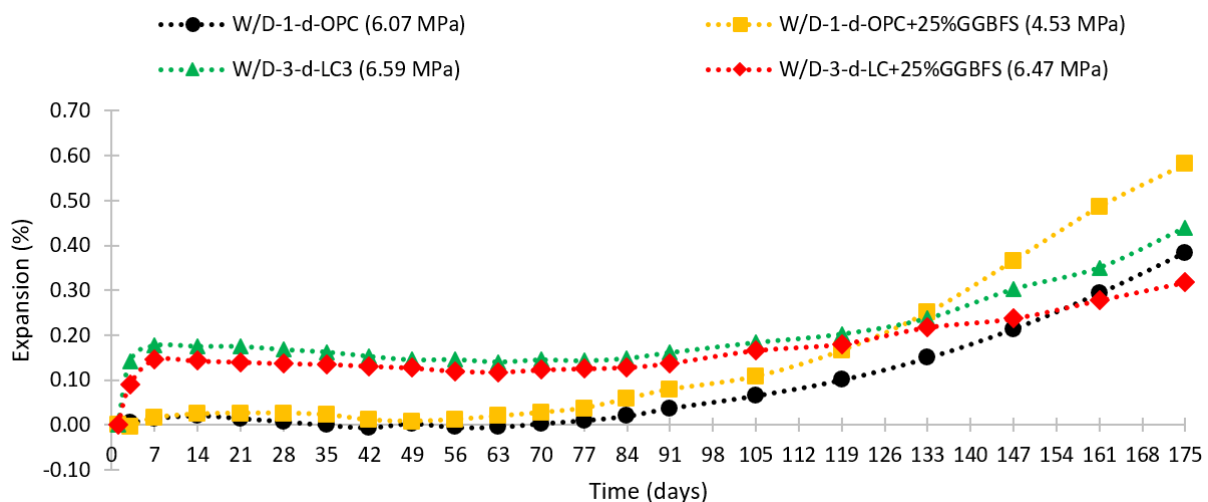

Figure 4.17: Expansion characteristics of W/D mixtures submerged in sodium sulfate solution at an early age.

Similarly, having an initial growth of around 0.15% in expansion, mixtures containing LC3 systems also stayed stable until about 105 days which is a bit longer than that of OPC mixtures. The big difference in deterioration of LC3 occurred after approximately 4 months, showing 1.4 times in the variation at 175-day. Unlike OPC, the LC3 system benefits from the addition of GGBFS demonstrating a lower expansion in wetting and drying cycles that can be found in Figure 4.13 showing XRD results.

A comparison of sulfate attack in normal and wet-dry conditions for the samples submerged in 5% sodium sulfate solution at low compressive strength is showed in Figure 4.18. The results revealed that all mixtures in wet and dry cycles saw bigger expansion than that in continuous normal curing after 175 days from the start of the test (see Figure 4.18 a). This agrees with the conclusions of the Portland Cement Association that claimed a physical sulfate attack is more dangerous than a chemical attack (Zhutovsky & Douglas Hooton, 2017). The mechanism of damage is due to the high pressure caused by the cyclic change of thenardite into mirabilite during the crystallization process which takes place in the pores on the edge of samples (Neville, 2004).

Interestingly, in the beginning, the expansion values of OPC and OPC+25%GGBFS mixtures were lower in the condition of wet-dry compared to normal. Only, by the age of 133-day and 91-day, it surpassed for OPC and OPC+25%GGBFS mixtures (see Figure 4.18 b). The difference between normal and wet-dry conditions was calculated according to Eq. 4.2.

$$D_{exp}(\%) = \frac{(L_{wet-dry} - L_{normal})}{L_{normal}} \ x \ 100 \qquad (4.2)$$

where, D_{exp} = a difference percentage in the expansion of two conditions, $L_{wet-dry}$ = the expansion of mortar bar in a wet-dry SA condition, and L_{normal} = the expansion of the mortar bar in normal SA condition.

The expansion of LC3 containing specimens stayed in a comparable range for both conditions. The figure also depicts that the greatest difference of as much as nearly 5 times between two sulfate attack conditions was observed in OPC+25%GGBFS whereas the smallest is found to be OPC with about 35%. This might be related to the higher quantity of small pores which benefits from better capillary suction and greater surface area for drying in the pure OPC mixture than that in a combination of GGBFS (Whittaker & Black, 2015).

Figure 4.19 presents the length change of the six mortar mixture bars with initial high strength submerged in 5% sodium sulfate solution in cycles of wetting and drying up to the age

of 91-day for OPC and 175-day for LC3 containing samples. From the general view, it can be concluded that bars with a high initial strength experienced a greater expansion in comparison with a low initial strength in a wet and dry conditions for all mixtures. Furthermore, unlike in the case of low strength condition, the pure LC3 mixtures expanded more than the OPC samples and all specimens were broken after 161-d (see Figure 4.20). These might be attributed to the larger number of pores in the low strength mortar bars that can help to reduce the effect of physical sulfate attack as discussed earlier.
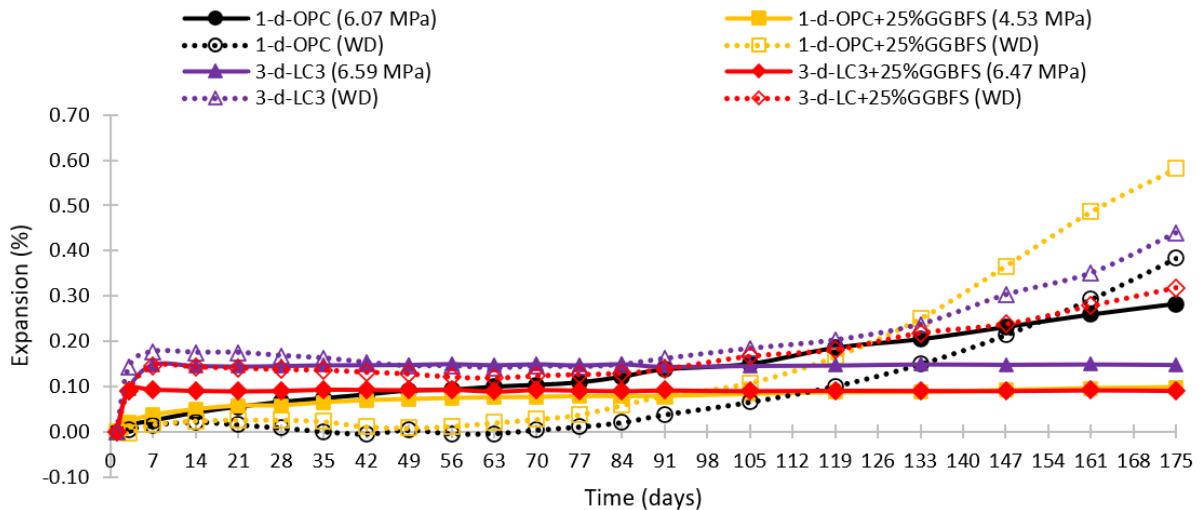

a) a combined view of samples exposed to sulfate attack at an early age in normal and wet-dry conditions
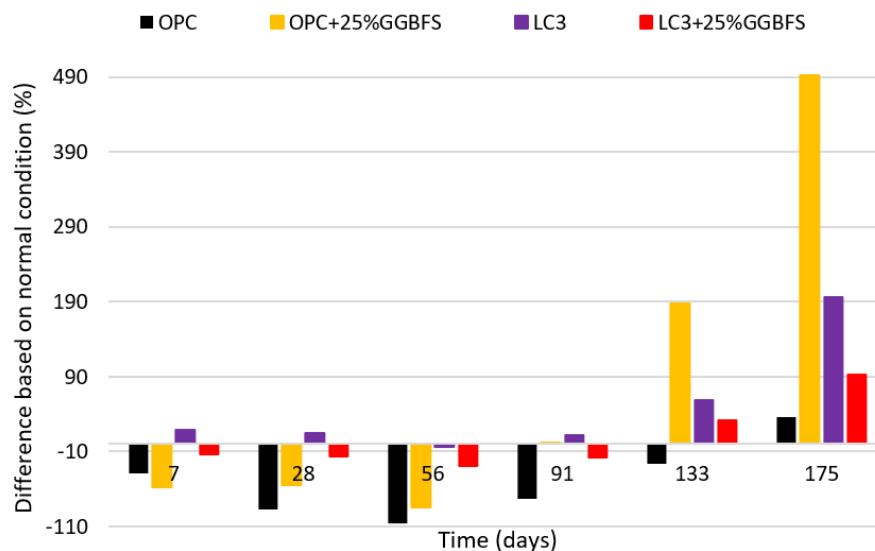

b) difference of expansion between normal and wet-dry conditions

Figure 4.18: Comparison of expansion characteristics of mixtures in normal and W/D curing conditions submerged in sodium sulfate solution at an early age.

The effect of GGBFS is seen clearly in both OPC and LC3 systems. In the latter, the level of GGBFS governed the severity of sulfate attack, making a huge difference in expansion by the age of 175-day. That is to say, more than 4 and 10 times smaller for 25% and 50% GGBFS addition. If to enlarge the graph, as shown in Figure 4.19 b, the effect of GGBFS for OPC is also a lot, resulting in about 4 times smaller expansion at 91-day. Furthermore, the influence of wetting and drying on expansion characteristics compared to the normal condition is obvious and showed many times of greater value for all mixtures. That supports the results of low strength mixtures previously discussed.
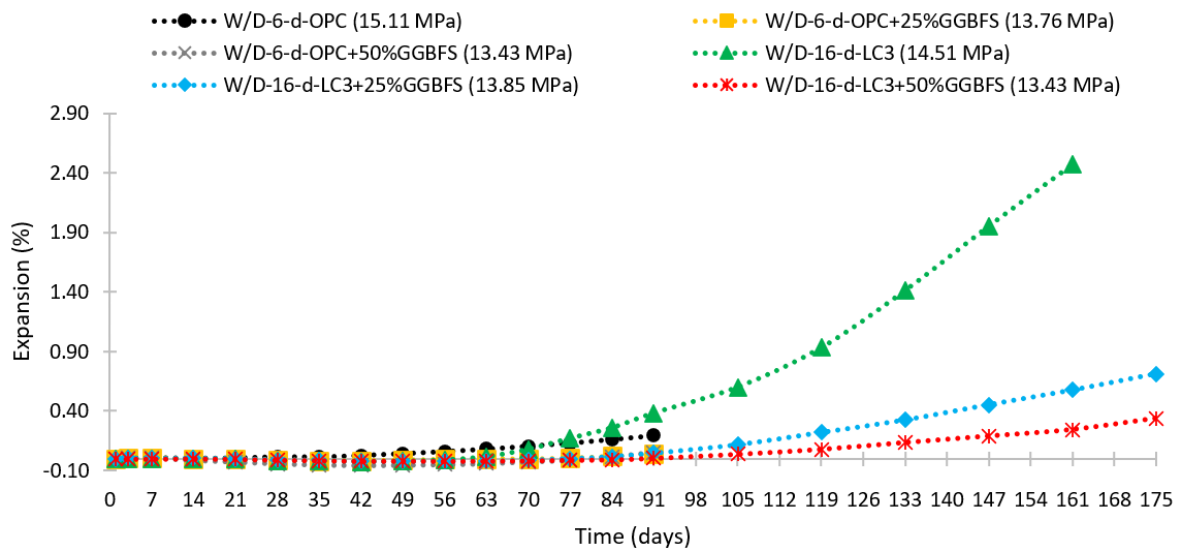
a)   a general view
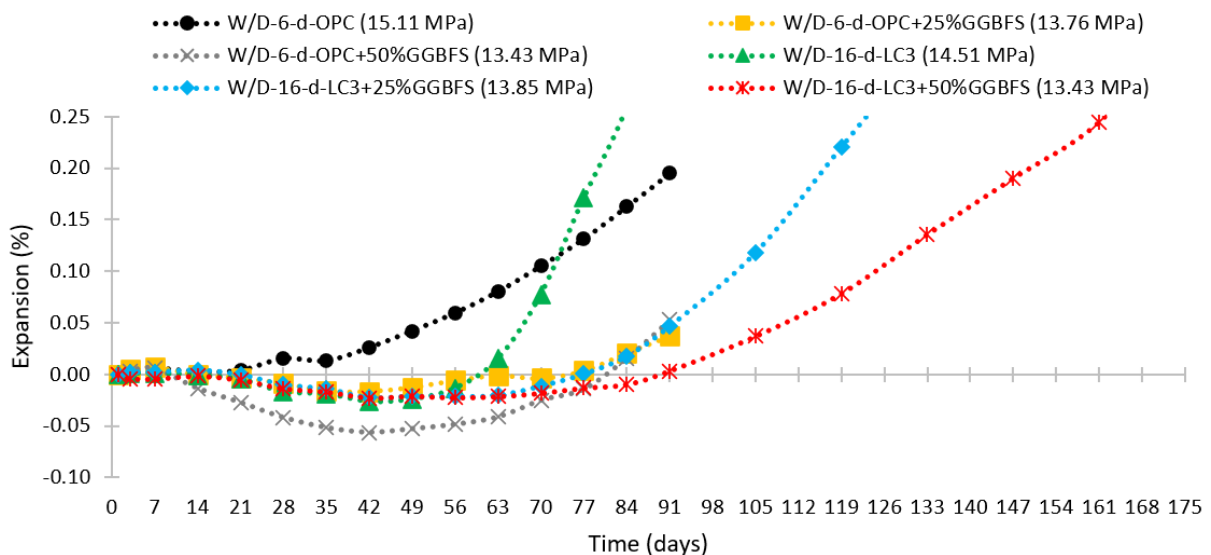
b)   an enlarged view

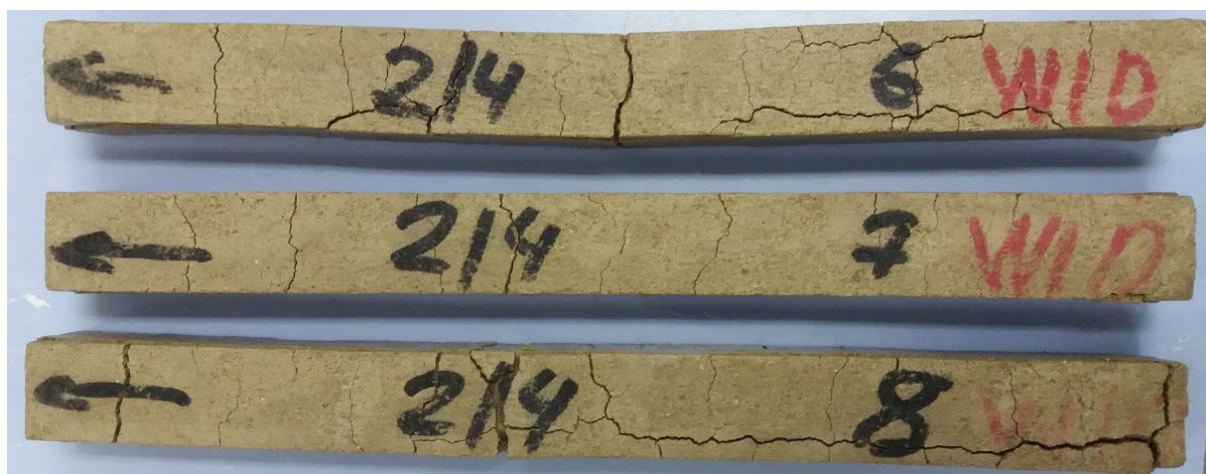***Figure 4.19: Expansion characteristics of W/D mixtures submerged in sodium sulfate solution with initial high strength.***

Figure 4.20: Deterioration degree of LC3 mixture after 161-d in W/D condition with initial high strength.

4.2.4 Relationship between sulfate attack resistance and porosity

Porosity that shows the ratio of pore spaces to the entire volume in hardened cement products and permeability that describes the interconnectivity of these pore spaces plays a key role in the performance of mortar and concrete with respect to durability concerns such as external sulfate attack. Since these and other factors, such as pore size and uniformity of their distribution throughout the concrete structure, are usually interrelated, the level of void ratio is extremely important to control and eliminate the deleterious effects of sulfate ions. Figure 4.21 illustrates the correlation of 175-day expansion characteristics of 6 different mixtures exposed to sulfate attack at a low strength and their void ratio upon the beginning of the test. If we look at the mixtures of LC3 and LC3+25%GGBFS at the level of within one mixture, the difference in the expansion level of 1-d and 3-d samples may be explained by the void ratio values. As expected, it is clear that a low degree of porosity results in less expansion in both cases.

However, it is not true for comparing different mixtures that show reverse results. Actually, the expansion is governed by the partial replacement level of cement with GGBFS at the intermixture levels. The effect of adding GGBFS to mitigate the sulfate attack is likely related to the pozzolanic reaction of GGBFS that goes by consuming portlandite which is the main provider of calcium ions to produce ettringite and gypsum (Z. Shi et al., 2019). Moreover, the reduction in expansion may be also caused by the improvement of pore size distribution upon adding GGBFS (Y. Yang et al., 2020).

A similar trend can be found for the composites that have high strength. It is presented in Figure 4.22 for all 6 blends comparing their void ratio and expansion at 91-day. As the ratio of GGBFS grows from 0% to 25% and 50%, both porosity and expansion decrease for OPC. In

contrast, LC3 containing mixtures saw a bit of fluctuation since their value too low and negligible (under 0.005%). The expansion characteristics for the entire period show it clearly which can be found in Figure 4.15 in the section of 4.2.1.
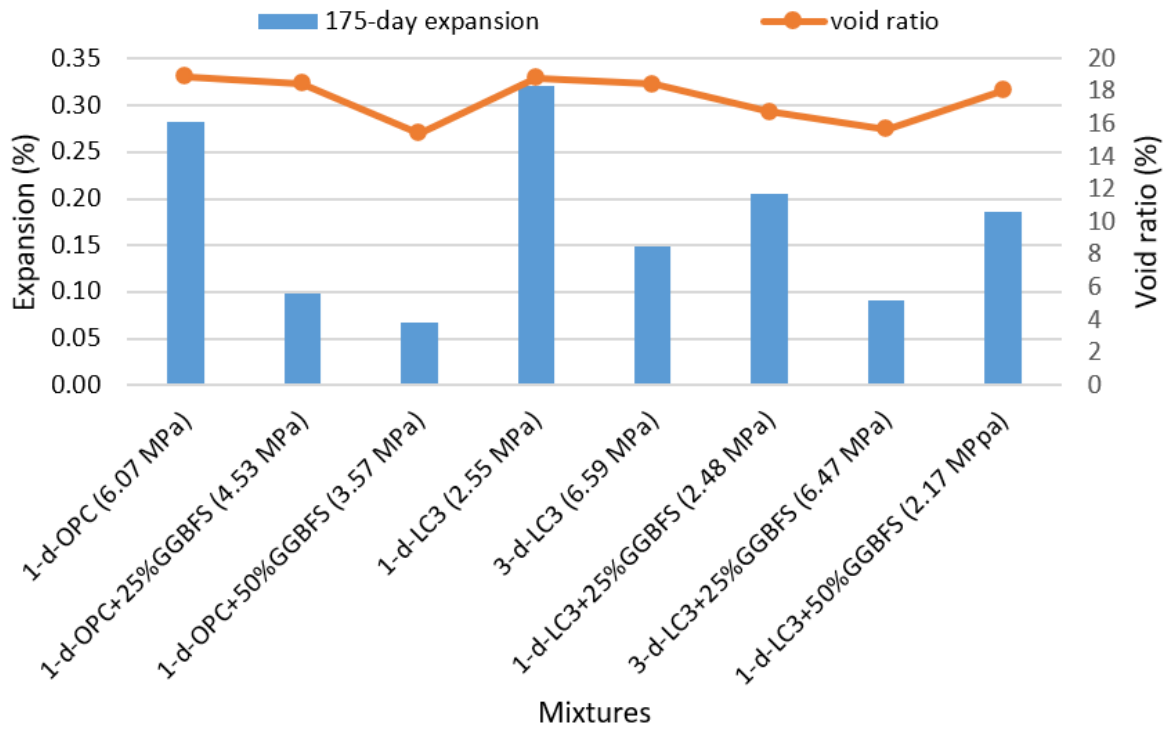

Figure 4.21: Relationship between expansion and void ratio of mixtures tested against sulfate attack with low initial strength.
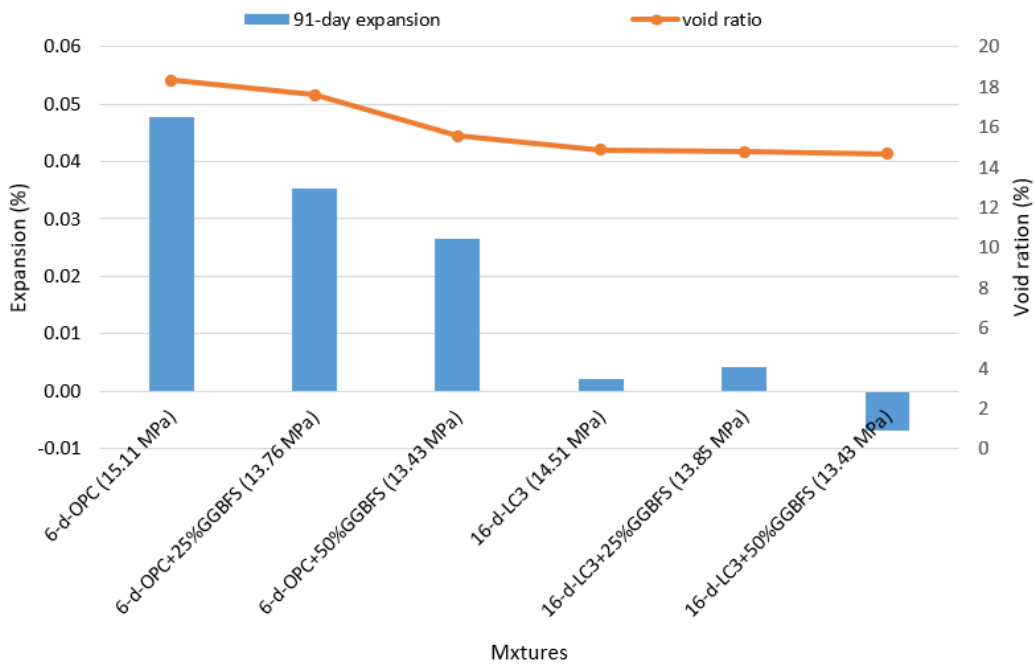

Figure 4.22: Correlation between sulfate attack expansion and void ratio of mortar mixtures with high initial strength.

4.2.5 Relationship between sulfate attack resistance and compressive strength

It is well known that the initial strength of samples testing for external sulfate attack is one of the primary parameters to determine the performance of mixtures. The comparison of expansion data with the samples' initial compressive strength is presented in Figure 4.23 for OPC contained mixtures up to the age of 3 months and for blends made from LC3 with/without GGBFS by 175-day.
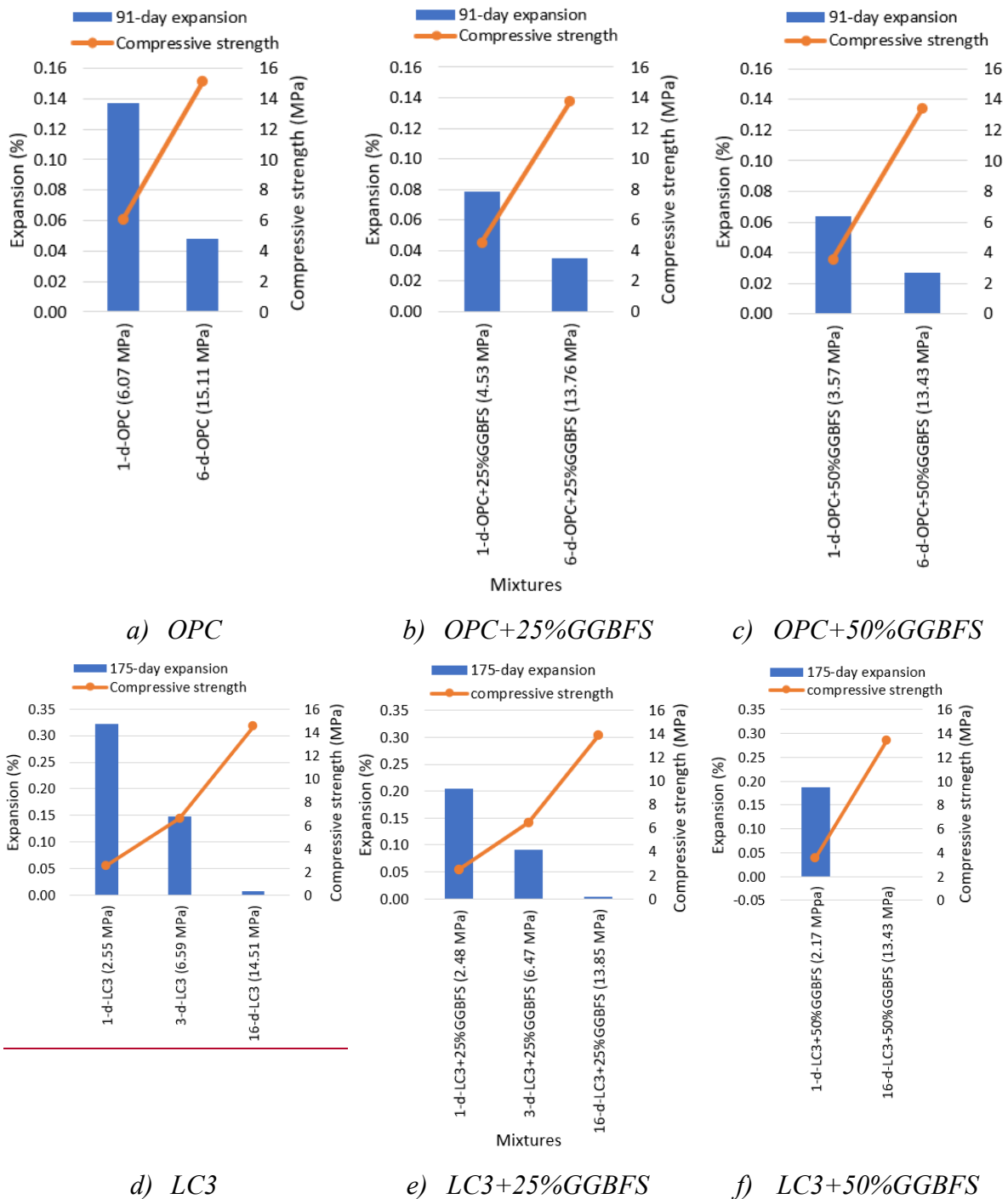

a) OPC   b) OPC+25%GGBFS   c) OPC+50%GGBFS

d) LC3   e) LC3+25%GGBFS   f) LC3+50%GGBFS

Figure 4.23: Effect of the initial strength of mixtures on expansion.

From the figure, it is obvious that the expansion of mortar bars decreases following the strength enhancement. That is attributed to the higher density and lower porosity of these specimens according to their strength that does not allow the sulfate ions to penetrate inside as discussed in Chapter 4.1.1.

In addition, curing for a long time before the sulfate attack gives a longer time for supplementary cementitious materials such as GGBFS to improve the chemical composition of composites. In other words, during the curing time, there happens secondary pozzolanic reaction that consumes more amount of calcium hydroxide that is susceptible to sulfate ions resulting in more CSH structure (Chidiac & Panesar, 2008; Maier & Durham, 2012; C. Shi & Qian, 2000).

Additional curing can be beneficial for LC3 mixtures too. For example, as a result of reaction due to aluminum oxide from calcined clay and calcite from limestone, additional aluminate hydrates are formed, which is a new phase (Antoni et al., 2012; Yuvaraj Dhandapani & Santhanam, 2017; K. Scrivener et al., 2018). This and calcined clays, which are very reactive, form dense hydration products consuming Portlandite (Y. Dhandapani et al., 2018; Yuvaraj Dhandapani & Santhanam, 2017).

4.2.6 Relationship between sulfate attack resistance and weight change

Figure 4.24 presents the relationship between expansion and weight change of mortar bar. The mass of all mixtures has continuously grown over time, which indicates that there is no spalling yet and supports the expansion data. The increase in the mass may be attributed to the formation of ettringite in the pores of mortar mixtures.

Interestingly, there is a good linear correlation between the length change of mortar and their weight change during the period of 6 months for LC3 mixtures, whereas the mortars made from OPC have shown much less relationship. In general, pure OPC mixture has an exponential function in the expansion characterization.

With an increase in compressive strength, the length change of mortar bars attacked by sulfate solution in normal curing conditions becomes less related to their mass change for composites made from LC3 systems (see Figure 4.25). Unlike the low strength specimens, this change is attributed to the very low expansion (almost none) values of LC3 blends over the whole period of time which makes the two variables unrelated. On the other hand, mortar bar compounds made from OPC with and without GGBFS have experienced a higher linear relationship in weight and length change showing an R^2 value of about 0.8.
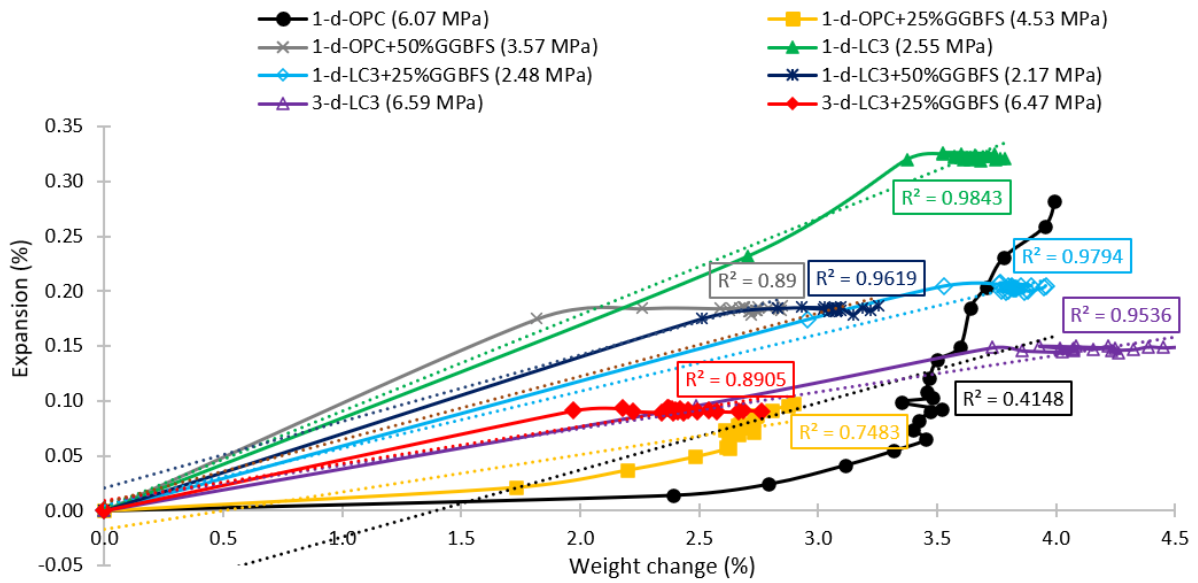
Figure 4.24: Relationship between expansion and weight change of mortar bars submerged in sodium sulfate solution at an early age.

Figure 4.25: Relationship between expansion and weight change of mortar bars submerged in sodium sulfate solution with initial high strength.

However, blends subjected to sulfate attack at an early age by wetting and drying conditions have shown different values, except for the LC3+25%GGBFS composites (see Figure 4.26). For example, the correlation between weight change and expansion for pure LC3 and OPC+25%GGBFS mixtures dropped considerably by nearly 0.3 and 0.2 in R^2, respectively. Nevertheless, it is worth mentioning that OPC has demonstrated a better correlation after wet-dry cycles rather than normal curing. Specimens tested against sulfate attack at a later age with

higher strength in drying and wetting cycles showed a good correlation only for pure OPC as well as LC3+25%GGBFS while others demonstrated an R^2 value of less than 0.7 (see Figure 4.27).
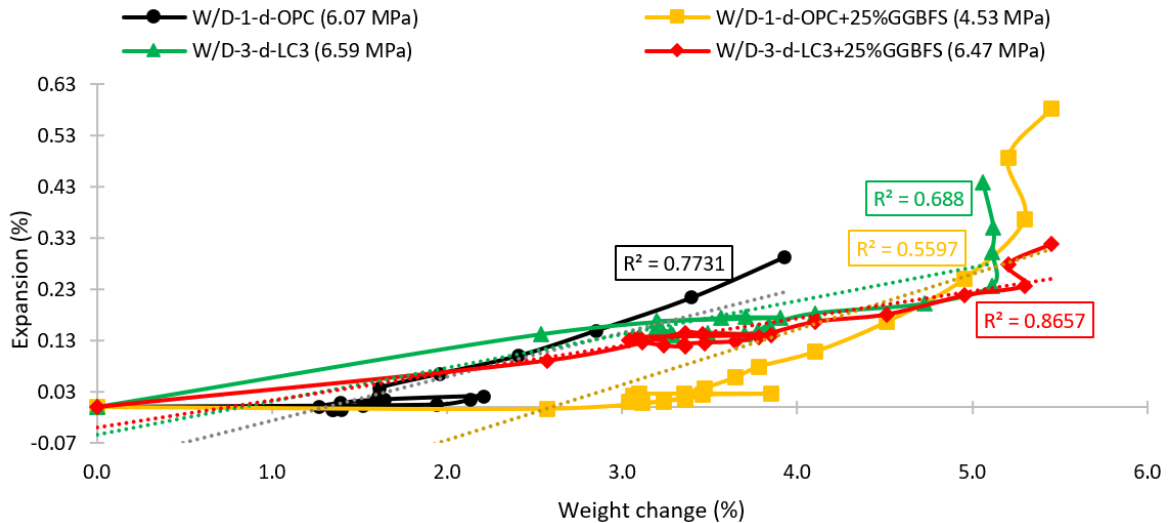
Figure 4.26: Relationship between expansion and weight change of W/D mortar bars submerged in sodium sulfate solution at an early age.
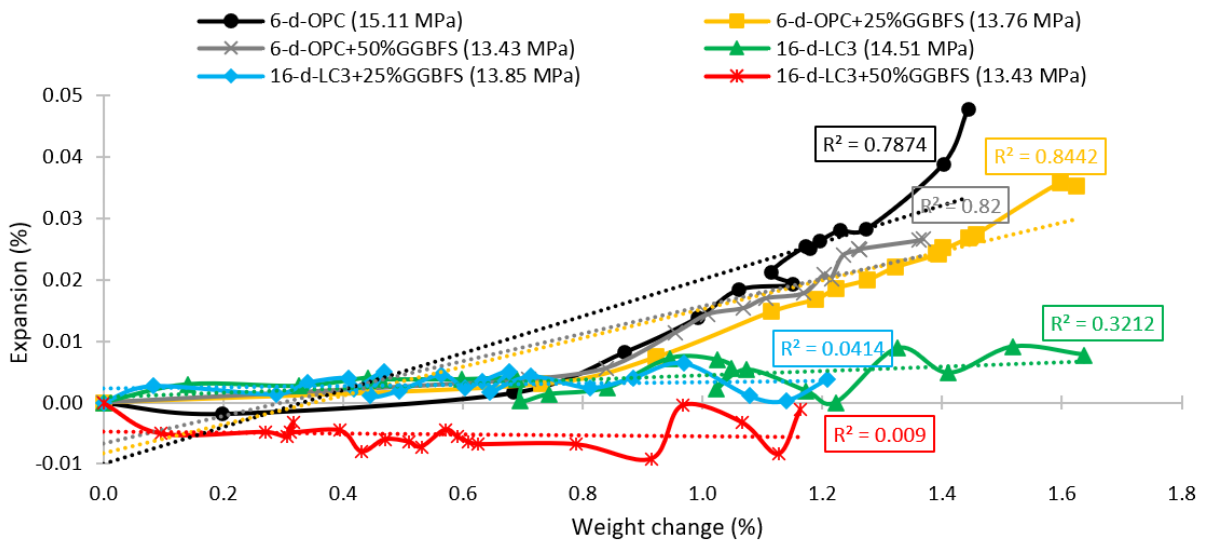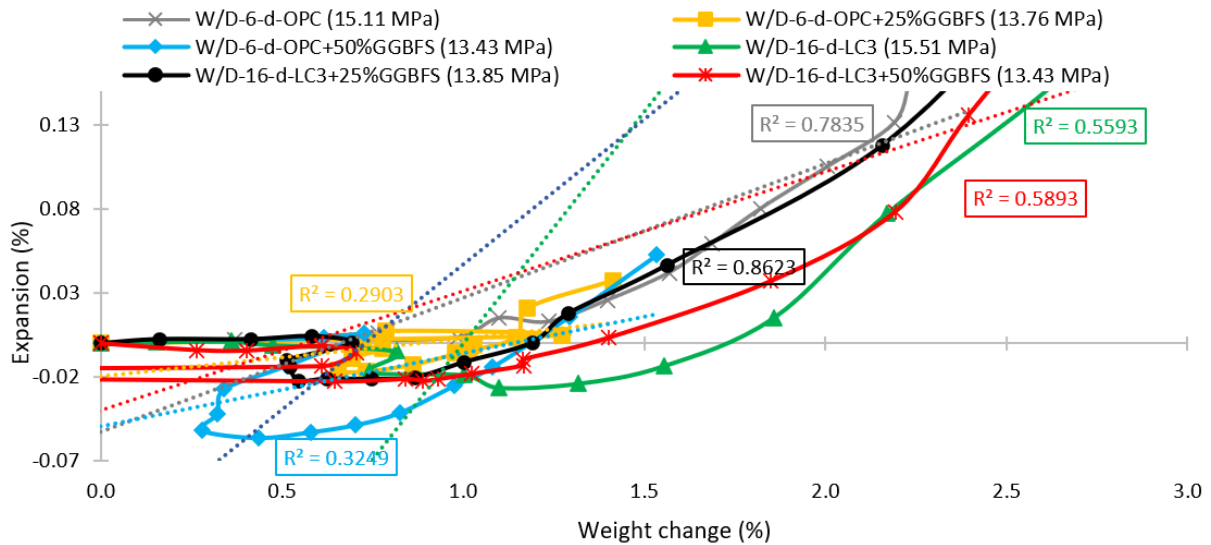

Figure 4.27: Relationship between expansion and weight change of W/D mortar bars submerged in sodium sulfate solution with initial high strength.

4.2.7 Relationship between sulfate attack resistance and dielectric constant

The electrical properties of hydration products are depended on the composition and proportion of their constituents. Generally, the primary components of mortar and concrete have low relative dielectric constant values (less than 10) except for free water that has at around

80 (S. I. Lee & Zollinger, 2012). As a result, the content of free water inside the sample usually governs the behavior of mortar with respect to electrical performance. (Shen et al., 2016) reported that properties such as dielectric constant, free water level, and the number of capillary pores are interrelated.

Therefore, to some extent, the performance of composites made from OPC cement against sulfate attack tested at an early age can be described by their correlation with the change in dielectric properties of mortar. In other words, the value of the dielectric constant drops as the degree of expansion rises. As it can be seen from Figure 4.28, there is a good linear relationship for OPC containing samples which grow further upon the addition of GGBFS from 0.74 to 0.89 and 0.93 in R^2 for 25% and 50% replacement levels, respectively. However, it should be noted that the slope of the linear correlation line decreases by growth in GGBFS content. This is probably attributed to the low content of alite that delays the level of hydration and better pore refinement that decreases the level of permeability, thus expansion (Maier & Durham, 2012).

Figure 4.28: Relationship between expansion and dielectric constant of mixtures made from OPC submerged in sodium sulfate solution at an early age.

The relationship between the length change of mortar bars and dielectric constant is different for blends containing LC3. Unlike OPC mixtures, they do not have linear correlation but rather polynomial (see Figure 4.29). This may be because of early pore refinement of

mixtures by 7 days (Yuvaraj Dhandapani & Santhanam, 2017) that resulted in no expansion at later ages. Nevertheless, the effect of GGBFS remains the same as in the case of OPC.
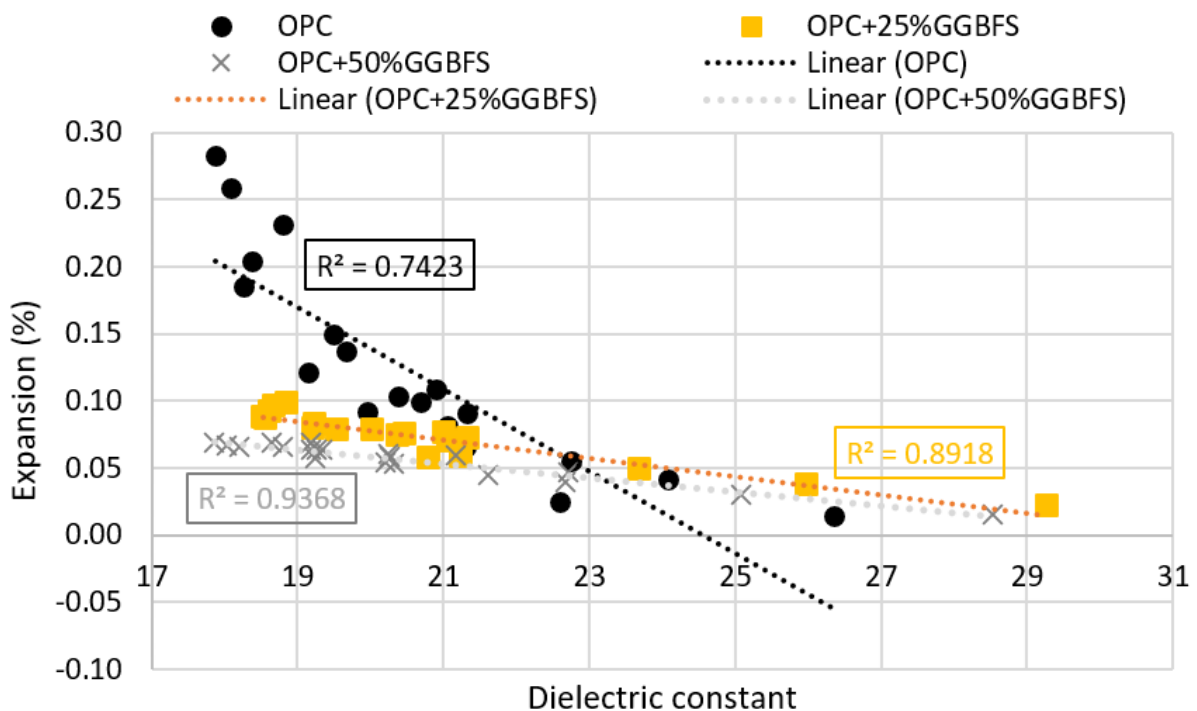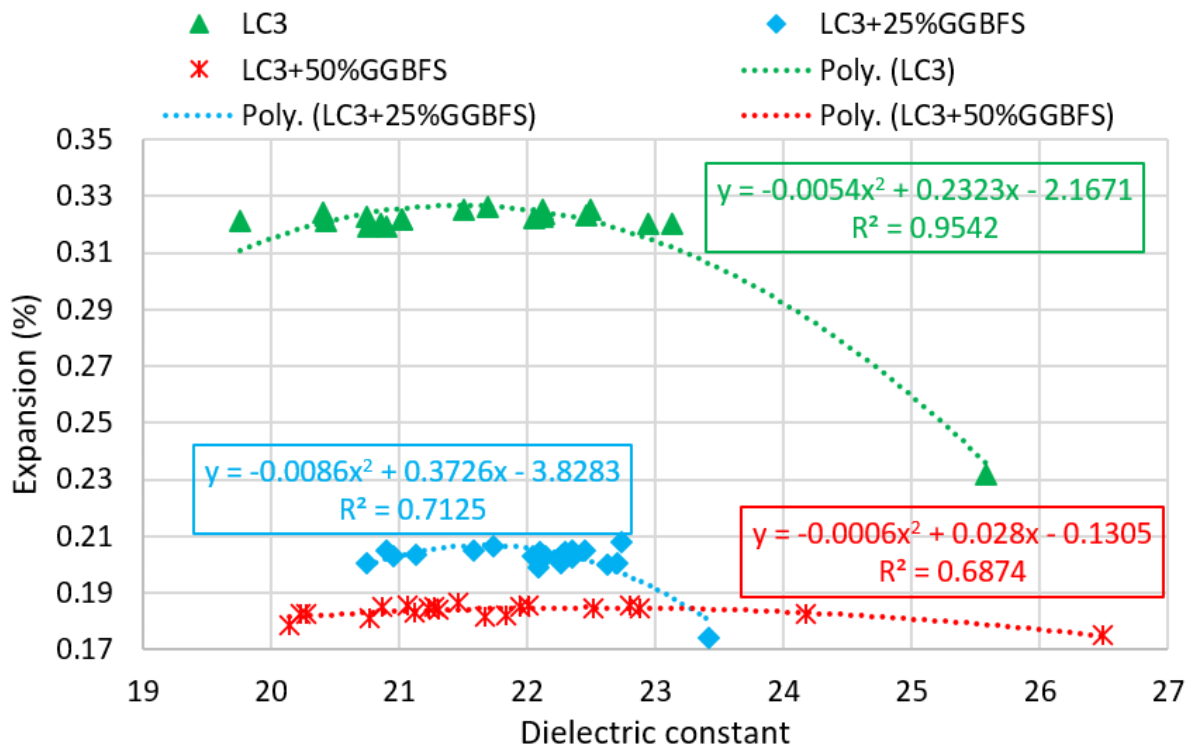

Figure 4.29: Relationship between expansion and dielectric constant of mixtures made from the LC3 system submerged in sodium sulfate solution at an early age.

Chapter 5 – Conclusion

5.1 General

In the present study, mechanical and physical properties of hardened OPC, LC3, and GGBFS-contained mortar mixtures such as void ratio, density, drying shrinkage, dielectric constant, and compressive strength were evaluated. Furthermore, their performance against external sulfate attack at early and late ages, based on their strength development, was investigated in 5% Na_2SO_4 solution for different conditions, namely normal and wet-dry cycles. Based on the results up to approximately 6 months, the following conclusions can be drawn:

1) Drying shrinkage test started after 1-d curing revealed that pure LC3 and OPC mixture bars contracted by a comparable value of approximately 0.175% in length change while the addition of GGBFS in the amount of 25% and 50% induced further increase.

2) Drying shrinkage of the designed 6 mixtures can be determined by the correlation with weight change.

3) Determination of dielectric constant demonstrated that all composites experience a downward trend over time indicating the level of hydration, thus pore structure development. Furthermore, the value is higher in sulfate attack than in lime-water curing.

4) The compressive strength of OPC mixtures with/without GGBFS is roughly 1.5 times higher than that of LC3 mixtures regardless of curing age (up to 175 days).

5) Mixtures exposed to Na_2SO_4 solution have higher compressive strength than water-cured mixtures up to 175-day irrespective of cement type and the incorporation of GGBFS.

6) The sulfate-induced expansion of LC3 mixtures after 1-d initial curing is higher than that of the OPC mixture regardless of the addition of GGBFS. However, at the roughly same strength of under 7 MPa, the LC3 mixture showed about two times lower expansion than the pure OPC whereas the addition of 25% GGBFS demonstrated a comparable result for both types of cement.

7) Expansion of mortar bars made from LC3 regardless of GGBFS content makes a plateau after a rapid increase up to 7 days at low initial strength, while the expansion of OPC mixture keeps increasing throughout the period.

8) At high initial strength of about 14 MPa, expansion characteristics of mixtures containing LC3 fluctuated below 0.01% throughout the period of up to 175-d while the

OPC-containing mixtures saw an upward trend reaching nearly 0.05% at only 91-d in the case of the pure OPC sample although the incorporation of GGBFS resulted in a decrease of that value.

9) During the sulfate attack in the wet-dry condition, the LC3 mixture had more expansion than the OPC one for both low and high initial strength.

10) Sulfate attack is more severe in wet-dry conditions than in the case of conventional normal exposure.

11) The addition of GGBFS to OPC or LC3 mixture provides a synergistic effect on reducing the expansion due to sulfate attack.

12) There is a good linear correlation between expansion and weight change of the mixtures over the indicated period.

5.2 Limitation and future recommendation

The used American standard has been criticized for the limitations due to the facts ignored in the test methods. For example, the solutions required for the test have a much higher concentration for lab tests than those actually found in natural fields which causes gypsum formation as well as ettringite that probably cannot be found in nature. Moreover, in lab tests, mostly only one pure type of sulfate source is used but in the actual application, there might be a combination of several. Finally, as the main indicator of sulfate attack, the standard only considers the level of expansion whereas other factors such as softening, decohesion, and ultimately degradation of concrete mixtures are not taken into account. In other words, other important indicators that can describe the sulfate attack damage like strength, elastic modulus, and weight change are ignored (Whittaker & Black, 2015).

This study result is based on approximately only 6 months of data. Therefore, all samples were not broken and the test can be continued. Moreover, the used LC3 systems showed poor quality in compressive strength which is much lower than that of OPC. Despite that, according to the study results, LC3 containing mixtures demonstrated an expansion value of below 0.01%. Therefore, it can be used as high sulfate resistance cement.

Bibliography/References

Al-Akhras, N. M. (2006). Durability of metakaolin concrete to sulfate attack. *Cement and Concrete Research*, *36*(9), 1727–1734. https://doi.org/10.1016/j.cemconres.2006.03.026

Andrade, C., Blanco, V. M., Collazo, A., Keddam, M., Nóvoa, X. R., & Takenouti, H. (1999). Cement paste hardening process studied by impedance spectroscopy. *Electrochimica Acta*, *44*(24), 4313–4318. https://doi.org/10.1016/S0013-4686(99)00147-4

Antoni, M., Rossen, J., Martirena, F., & Scrivener, K. (2012). Cement substitution by a combination of metakaolin and limestone. *Cement and Concrete Research*, *42*(12), 1579–1589. https://doi.org/10.1016/j.cemconres.2012.09.006

ASTM C1012/C1012M. (2015). Standard test method for length change of hydraulic-cement mortars exposed to a sulfate solution. *ASTM International, West Conshohocken, PA*, *11*, 5–9. https://doi.org/10.1520/C1012

ASTM C109/109M. (2016). Standard test method for compressive strength of hydraulic cement mortars (Using 2-in. or cube specimens). *Annual Book of ASTM Standards*, 1–10. https://doi.org/10.1520/C0109

ASTM C128. (2003). Standard Test Method for Density , Relative Density (Specific Gravity), and Absorption 127/C. *ASTM International*, *88*(October 2001), 1–6.

ASTM C1437. (2013). C1437 - Standard test method for flow of hydraulic cement mortar. *ASTM International*, 1–2. https://www.astm.org/Standards/C1437

ASTM C150/C150M. (2020). *ASTM C150_C150M.15210*. *i*(Reapproved), 1–3. https://doi.org/10.1520/C0150

ASTM C157/C157M. (2017). Standard Test Method for Length Change of Hardened Hydraulic-Cement Mortar and. *Annual Book of ASTM Standards*, *04*, 1–7. https://doi.org/10.1520/C0157

ASTM C305. (2011). Standard Practice for Mechanical Mixing of Hydraulic Cement Pastes and Mortars of Plastic Consistency. *ASTM Lnternational*, 1–3.

ASTM C490/C490M. (2017). Standard practice for use of apparatus for the determination of length change of hardened cement paste , mortar , and concrete. *ASTM International*, 1–5. https://doi.org/10.1520/C0490

ASTM C494/C494M. (2013). ASTM C494/C494M-04: Standard Specification for Chemical Admixtures for Concrete. *American Society for Testing and Materials.*, *February*, 15–17.

ASTM C642. (1997). Standard Test Method for Density, Absorption, and Voids in Hardened Concrete, ASTM International, United States. *Annual Book of ASTM Standards*, *March*, 1–3.

Bensted, J. (1983). *Hydration of Portland cement*. Pergamon.

Bescher, E., Rice, E. K., Ramseyer, C., & Roswurm, S. (2016). Sulfate resistance of calcium sulphoaluminate cement. *Journal of Structural Integrity and Maintenance*, *1*(3), 131–139. https://doi.org/10.1080/24705314.2016.1211235

Chidiac, S. E., & Panesar, D. K. (2008). Evolution of mechanical properties of concrete containing ground granulated blast furnace slag and effects on the scaling resistance test at 28 days. *Cement and Concrete Composites*, *30*(2), 63–71. https://doi.org/10.1016/j.cemconcomp.2007.09.003

Chung, K. L., Yuan, L., Ji, S., Sun, L., Qu, C., & Zhang, C. (2017). Dielectric characterization of Chinese standard concrete for compressive strength evaluation. *Applied Sciences (Switzerland)*, *7*(2). https://doi.org/10.3390/app7020177

Crossin, E. (2015). The greenhouse gas implications of using ground granulated blast furnace slag as a cement substitute. *Journal of Cleaner Production*, *95*, 101–108. https://doi.org/10.1016/j.jclepro.2015.02.082

Darquennes, A., Rozière, E., Khokhar, M. I. A., Turcry, P., Loukili, A., & Grondin, F. (2012). Long-term deformations and cracking risk of concrete with high content of mineral additions. *Materials and Structures/Materiaux et Constructions*, *45*(11), 1705–1716. https://doi.org/10.1617/s11527-012-9867-5

Dhandapani, Y., Vignesh, K., Raja, T., & Santhanam, M. (2018). Development of the Microstructure in LC3 Systems. *Calcined Clays for Sustainable Concrete*, *16*, 131–140.

Dhandapani, Yuvaraj, Sakthivel, T., Santhanam, M., Gettu, R., & Pillai, R. G. (2018). Mechanical properties and durability performance of concretes with Limestone Calcined Clay Cement (LC3). *Cement and Concrete Research*, *107*(July 2017), 136–151. https://doi.org/10.1016/j.cemconres.2018.02.005

Dhandapani, Yuvaraj, & Santhanam, M. (2017). Assessment of pore structure evolution in the limestone calcined clay cementitious system and its implications for performance. *Cement and Concrete Composites*, *84*, 36–47. https://doi.org/10.1016/j.cemconcomp.2017.08.012

El-Hachem, R., Rozière, E., Grondin, F., & Loukili, A. (2012). Multi-criteria analysis of the mechanism of degradation of Portland cement based mortars exposed to external sulphate attack. *Cement and Concrete Research*, *42*(10), 1327–1335. https://doi.org/10.1016/j.cemconres.2012.06.005

Farfan, J., Fasihi, M., & Breyer, C. (2019). Trends in the global cement industry and opportunities for long-term sustainable CCU potential for Power-to-X. *Journal of Cleaner Production*, *217*, 821–835. https://doi.org/10.1016/j.jclepro.2019.01.226

Gruyaert, E., Van Den Heede, P., & De Belie, N. (2013). Carbonation of slag concrete: Effect of the cement replacement level and curing on the carbonation coefficient - Effect of carbonation on the pore structure. *Cement and Concrete Composites*, *35*(1), 39–48. https://doi.org/10.1016/j.cemconcomp.2012.08.024

Khatri, R. P., Sirivivatnanon, V., & Yang, J. L. (1997). Role of permeability in sulphate attack. *Cement and Concrete Research*, *27*(8), 1179–1189. https://doi.org/10.1016/S0008-8846(97)00119-1

Lee, J. H., & Yoon, Y. S. (2015). The effects of cementitious materials on the mechanical and durability performance of high-strength concrete. *KSCE Journal of Civil Engineering*, *19*(5), 1396–1404. https://doi.org/10.1007/s12205-014-0658-0

Lee, S. I., & Zollinger, D. G. (2012). Estimating Volume Fraction of Free Water in Hardening Concrete by Interpretation of Dielectric Constant. *Journal of Materials in Civil Engineering*, *24*(2), 159–167. https://doi.org/10.1061/(asce)mt.1943-5533.0000371

Li, C., Sun, H., & Li, L. (2010). A review: The comparison between alkali-activated slag (Si + Ca) and metakaolin (Si + Al) cements. *Cement and Concrete Research*, *40*(9), 1341–1349. https://doi.org/10.1016/j.cemconres.2010.03.020

Lu, J. X., & Poon, C. S. (2018). Use of waste glass in alkali activated cement mortar. *Construction and Building Materials*. https://doi.org/10.1016/j.conbuildmat.2017.11.080

Lv, X., Dong, Y., Wang, R., Lu, C., & Wang, X. (2020). Resistance improvement of cement mortar containing silica fume to external sulfate attacks at normal temperature. *Construction and Building Materials*, *258*(June), 119630. https://doi.org/10.1016/j.conbuildmat.2020.119630

Maier, P. L., & Durham, S. A. (2012). Beneficial use of recycled materials in concrete mixtures. *Construction and Building Materials*, *29*, 428–437. https://doi.org/10.1016/j.conbuildmat.2011.10.024

Maraghechi, H., Avet, F., Wong, H., Kamyab, H., & Scrivener, K. (2018). Performance of Limestone Calcined Clay Cement (LC3) with various kaolinite contents with respect to chloride transport. *Materials and Structures/Materiaux et Constructions*, *51*(5). https://doi.org/10.1617/s11527-018-1255-3

Martirena, F., Diáz, E., Rocha, D., Maraghechi, H., & Scrivener, K. (2018). Performance of concrete made with a calcined clay-limestone-portland cement exposed to natural conditions. *6th International Conference on Durability of Concrete Structures, ICDCS 2018*, *July*, 244–247.

Meyer, C. (2009). The greening of the concrete industry. *Cement and Concrete Composites*, *31*(8), 601–605. https://doi.org/10.1016/j.cemconcomp.2008.12.010

Monteiro, P. J. M., & Kurtis, K. E. (2003). Time to failure for concrete exposed to severe sulfate attack. *Cement and Concrete Research*, *33*(7), 987–993. https://doi.org/10.1016/S0008-8846(02)01097-9

Neville, A. (2004). The confused world of sulfate attack on concrete. *Cement and Concrete Research*, *34*(8), 1275–1296. https://doi.org/10.1016/j.cemconres.2004.04.004

Özbay, E., Erdemir, M., & Durmuş, H. I. (2016). Utilization and efficiency of ground granulated blast furnace slag on concrete properties - A review. *Construction and Building Materials*, *105*, 423–434. https://doi.org/10.1016/j.conbuildmat.2015.12.153

Piatak, N. M., Parsons, M. B., & Seal, R. R. (2015). Characteristics and environmental aspects of slag: A review. In *Applied Geochemistry* (Vol. 57). Elsevier Ltd. https://doi.org/10.1016/j.apgeochem.2014.04.009

Pierkes, R., Schulze, S. E., & Rickert, J. (2018). Durability of concretes made with calcined clay composite cements. *RILEM Bookseries*, *16*, 366–371. https://doi.org/10.1007/978-94-024-1207-9_59

Pillai, R. G., Gettu, R., Santhanam, M., Rengaraju, S., Dhandapani, Y., Rathnarajan, S., & Basavaraj, A. S. (2019). Service life and life cycle assessment of reinforced concrete systems with limestone calcined clay cement (LC3). *Cement and Concrete Research*, *118*(July), 111–119. https://doi.org/10.1016/j.cemconres.2018.11.019

Ramezanianpour, A. M. (2012). Sulfate Resistance and Properties of Portland - Limestone Cements. *University of Toronto*, 185.

Ramezanianpour, A. M., & Hooton, R. D. (2013). Sulfate resistance of Portland-limestone cements in combination with supplementary cementitious materials. *Materials and Structures/Materiaux et Constructions*, *46*(7), 1061–1073. https://doi.org/10.1617/s11527-012-9953-8

Scrivener, K. L., John, V. M., & Gartner, E. M. (2018). Eco-efficient cements: Potential economically viable solutions for a low-CO2 cement-based materials industry. *Cement and Concrete Research*, *114*(March), 2–26. https://doi.org/10.1016/j.cemconres.2018.03.015

Scrivener, K., Martirena, F., Bishnoi, S., & Maity, S. (2018). Calcined clay limestone cements (LC3). *Cement and Concrete Research*, *114*(August 2017), 49–56. https://doi.org/10.1016/j.cemconres.2017.08.017

Sharp, J. H., Gartner, E. M., & Macphee, D. E. (2010). Novel cement systems (sustainability). Session 2 of the fred glasser cement science symposium. *Advances in Cement Research*, *22*(4), 195–202. https://doi.org/10.1680/adcr.2010.22.4.195

Shen, P., & Liu, Z. (2019). Study on the hydration of young concrete based on dielectric property measurement. *Construction and Building Materials*, *196*, 354–361. https://doi.org/10.1016/j.conbuildmat.2018.11.150

Shen, P., Lu, L., He, Y., Wang, F., & Hu, S. (2016). Hydration monitoring and strength prediction of cement-based materials based on the dielectric properties. *Construction and Building Materials*, *126*, 179–189. https://doi.org/10.1016/j.conbuildmat.2016.09.030

Shi, C., & Qian, J. (2000). High performance cementing materials from industrial slags - A review. *Resources, Conservation and Recycling*, *29*(3), 195–207. https://doi.org/10.1016/S0921-3449(99)00060-9

Shi, Z., Ferreiro, S., Lothenbach, B., Geiker, M. R., Kunther, W., Kaufmann, J., Herfort, D., & Skibsted, J. (2019). Sulfate resistance of calcined clay – Limestone – Portland cements. *Cement and Concrete Research*, *116*(October 2018), 238–251. https://doi.org/10.1016/j.cemconres.2018.11.003

Skalny, J., Marchand, J., & Odler, I. (2002). Modern concrete technology series: Sulfate attack on concrete. In *Spon Press: Taylor & Francis* (Vol. 40, Issue 04).

Summerbell, D. L., Barlow, C. Y., & Cullen, J. M. (2016). Potential reduction of carbon emissions by performance improvement: A cement industry case study. *Journal of*

Cleaner Production, *135*, 1327–1339. https://doi.org/10.1016/j.jclepro.2016.06.155

Tian, W., & Han, N. (2017). Experiment Analysis of Concrete's Mechanical Property Deterioration Suffered Sulfate Attack and Drying-Wetting Cycles. *Advances in Materials Science and Engineering*, *2017*. https://doi.org/10.1155/2017/5673985

Whittaker, M., & Black, L. (2015). Current knowledge of external sulfate attack. *Advances in Cement Research*, *27*(9), 532–545. https://doi.org/10.1680/adcr.14.00089

Xie, Y., Tang, X., & Long, G. (2011). Experiment on cement-based materials with various compositions against sulfate attack. *Advanced Materials Research*, *168–170*, 94–98. https://doi.org/10.4028/www.scientific.net/AMR.168-170.94

Yang, S., Zhongzi, X., & Mingshu, T. (1996). The process of sulfate attack on cement mortars. *Advanced Cement Based Materials*, *4*(1), 1–5. https://doi.org/10.1016/s1065-7355(96)90057-7

Yang, Y., Zhan, B., Wang, J., Zhang, Y., & Duan, W. (2020). Damage evolution of cement mortar with high volume slag exposed to sulfate attack. *Construction and Building Materials*, *247*, 118626. https://doi.org/10.1016/j.conbuildmat.2020.118626

Zhang, W., Gong, S., & Kang, B. (2017). Surface Corrosion and Microstructure Degradation of Calcium Sulfoaluminate Cement Subjected to Wet-Dry Cycles in Sulfate Solution. *Advances in Materials Science and Engineering*, *2017*. https://doi.org/10.1155/2017/1464619

Zhutovsky, S., & Douglas Hooton, R. (2017). Accelerated testing of cementitious materials for resistance to physical sulfate attack. *Construction and Building Materials*, *145*, 98–106. https://doi.org/10.1016/j.conbuildmat.2017.03.239